The Association of the Elevated Mixed Layer with Significant Severe Weather Events in the Northeastern United States

PETER C. BANACOS

NOAA/NWS/Weather Forecast Office, Burlington, Vermont

MICHAEL L. EKSTER

NOAA/NWS/Weather Forecast Office, Taunton, Massachusetts

Submitted: 5 October 2009
Revised: 24 January 2010

Accepted as an Article to *Weather and Forecasting*

Corresponding author address: Peter C. Banacos, NOAA/NWS/Weather Forecast Office, 1200 Airport Drive, South Burlington, VT 05403.

E-Mail: peter.banacos@noaa.gov

ABSTRACT

The occurrence of rare but significant severe weather events associated with elevated mixed-layer (EML) air in the northeastern United States is investigated herein. A total of 447 convective event days with one or more significant severe weather reports (where *significant* is defined as hail 2 in (5.1 cm) in diameter or greater, a convective gust of 65 kts (33 ms^{-1}) or greater, and/or a tornado of F2 or greater intensity) were identified from 1970 through 2006 during the warm season (May 1 through September 30). Of these, 34 event days (7.6%) were associated with identifiable EML air in regional rawinsondes preceding the event. Taken with two other noteworthy events in 1953 and 1969, a total of 36 significant severe weather events associated with EML air were studied via composite and trajectory analysis. Though a small percentage of the total, these 36 events comprise a noteworthy list of historically significant derechos and tornadic events to affect the northeastern United States.

It is demonstrated that plumes of EML air emanating from the Intermountain West in subsiding, anticyclonically curved flows can reinforce the capping inversion and maintain the integrity of the EML across the central United States over a few days. The EML plume can ultimately become entrained into a moderately fast westerly to northwesterly midtropospheric flow allowing for the plume's advection into the northeastern United States. Resultant thermodynamic conditions in the convective storm environment are similar to that more typically observed closer to the EML source region in the Great Plains of the United States.

In addition to composite and trajectory analysis, two case studies are employed to demonstrate salient and evolutionary aspects of the EML in such events. A lapse rate tendency equation is explored to put EML advection in context with other processes affecting lapse rate.

1. Introduction

During late spring and summer, it is common downstream of major mountain ranges to find evidence of displaced hot, dry, and deeply mixed boundary layer air which has moved with the prevailing horizontal flow over areas of lower terrain. Such an example is revealed in the juxtaposed soundings in Fig. 1, where the surface based mixed-layer extending upward to 450 mb at Albuquerque, New Mexico (station elevation 1620 m) has advected in a quasi-conservative manner to Dodge City, Kansas (station elevation 790 m), with nearly dry-adiabatic lapse rates present in the 700 – 450 mb layer. The horizontal advection of deeply-mixed boundary layer air off the elevated terrain is manifest as an *elevated mixed-layer* (EML) (Carlson and Ludlam 1968) and is a readily identified feature by convective forecasters dating back to the conceptual "type 1" (or "loaded gun") sounding as described by Fawbush and Miller (1954). The base of the EML lies atop an interface of strong static stability (the "capping" inversion), which – given a moist local boundary layer - creates convective inhibition for surface lifted parcels and allows for a strong buildup of convective available potential energy (CAPE), potentially prior to the initiation of deep moist convection. The EML is a contributor to the well known climatological maximum in severe weather occurrence across the Great Plains of the United States, and has been studied for its high frequency there (Carlson et al. 1983; Lanicci and Warner 1991; Lanicci and Warner 1997).

The frequency of *significant severe weather* (SIG SVR) (defined by the occurrence of hail $\geq$ 2 in (5.1 cm) in diameter, convective wind gusts $\geq$ 65 kts (33 ms^{-1}), and/or tornadoes of $\geq$ F2 intensity) over the northeastern United States (NEUS) is an order of magnitude less than across the central and southern Great Plains (Concannon et al. 2000; Doswell et al. 2005); a more northern latitude, and the absence of rich low-level moisture associated with parcel trajectories

from the Gulf of Mexico are important factors. In addition, the decreased frequency of the EML as a function of increased distance from the Intermountain West (Farrell and Carlson 1989) limits the ability to generate similarly large CAPE values across the eastern United States (Doswell and Bosart 2001). Likewise, operational experience suggests that the absence of steep mid-level lapse rates is a primary limiting factor for SIG SVR in the NEUS. While EML formation is well understood, the subsequent movement, evolution, and eventual destruction of the "EML plume" (defined as the horizontal extent of the EML) has received less attention.

Though rare, the intrusion of EML air and its influence on severe weather in the NEUS has been documented. Johns and Dorr (1996) examined 22 tornado episodes in eastern New York and New England from 1950-1991 and found evidence of modified EML air in three violent tornado cases occurring in westerly to northwesterly mid-level flow regimes. Farrell and Carlson (1989) documented the role of an EML in the generation of unusually large CAPE values, contributing to the severity of the 31 May 1985 tornado outbreak in the upper Ohio Valley. The same study showed a 4-year climatology of the "lid" (i.e., the capping inversion below the EML base), which indicated the occasional intrusion of the EML into the NEUS during the warm season (on the order of 1 day per month), and a relative maxima of the lid across the Great Plains. These studies were limited insofar as (1) they solely focused on tornadoes and not derechos or large hail events, and (2) they were performed prior to high-powered compositing techniques afforded by modern reanalysis datasets.

The motivation for this work was to catalog SIG SVR events, of any type, with an EML present in the NEUS. Furthermore, the goal was to then use composite and trajectory techniques to better understand the large-scale conditions and physical processes favorable for the unusually long downstream transport of the EML from the Intermountain West to the NEUS. We believe

this knowledge will provide forecasters with a framework to better anticipate EML associated SIG SVR events, leading to improved forecasts, warnings, and call-to-action statements commensurate with the threat posed to life and property.

The remainder of this paper is organized as follows. In Section 2, we present a lapse rate tendency equation, including a physical interpretation and scale analysis. Section 3 explains the observational and severe weather report data utilized for the composite and trajectory analyses, which follow in Section 4. Individual case studies are shown in Section 5. Finally, in Section 6, a concluding summary and ideas for future work are presented.

2. Lapse Rate Tendency Equation

a. Physical interpretation

The change in lapse rate as a result of downstream advection of the EML depicted in Fig. 1 is important in establishing the thermodynamic conditions needed for significant CAPE and large vertical parcel accelerations within severe thunderstorms. It is useful to have a theoretical framework for the local rate of change of lapse rate, $\frac{\partial \gamma}{\partial t}$, to understand the relevant physical processes before proceeding to the observational study. The lapse rate tendency equation is defined in (1) and derived in the appendix:

$$\frac{\partial \gamma}{\partial t} = \underbrace{-\frac{1}{c_p}\frac{\partial Q}{\partial z}}_{\mathbf{a}} \underbrace{-\mathbf{V}\cdot\nabla_h \gamma}_{\mathbf{b}} \underbrace{-w\frac{\partial \gamma}{\partial z}}_{\mathbf{c}} \underbrace{+\frac{\partial \mathbf{V}}{\partial z}\cdot\nabla_h T}_{\mathbf{d}} \underbrace{+\frac{\partial w}{\partial z}(\Gamma_d - \gamma)}_{\mathbf{e}} \qquad (1)$$

diabatic heating; horizontal lapse rate advection; vertical lapse rate advection; differential temperature advection; vertical stretching

where Q is the diabatic heating rate, $\mathbf{V}$ is the horizontal wind, w is the vertical velocity, Γ_d is the dry adiabatic lapse rate, and c_p is the specific heat at constant pressure. The terms on the right

hand side of (1) from left to right (and correspondingly illustrated in Fig. 2) are as follows. Term *a* is the *diabatic heating term*. For example, a decrease (an increase) in diabatic heating with height yields a steepening (lessening) lapse rate. Terms *b* and *c* are the *horizontal and vertical lapse rate advection term*s, respectively. Term *d* is the *differential temperature advection term*, which must be due to the ageostrophic part of the wind (since $\frac{\partial \mathbf{V}_g}{\partial z} \cdot \nabla_h T = 0$). For instance, a steepening (a lessening) of lapse rate would occur within a thermally indirect (direct) circulation. Lastly, Term *e* is the *vertical stretching term*, which is modulated by the instantaneous departure of the environmental lapse rate from the dry adiabatic value. If the environmental lapse rate is less than dry adiabatic, an increase (decrease) in upward (downward) vertical motion with height will lead to a steepening lapse rate.

b. Scale analysis

One can make assumptions as to the order of magnitude of terms in (1) for synoptic-scale motion away from fronts, jets, and areas of deep moist convection, as shown in Table 1. Since the undisturbed EML plume is isolated from boundary layer processes and largely void of moist thermodynamic processes, diabatic heating was estimated from studies of zonally averaged radiative heating rate in mid-latitudes (e.g., Peixoto and Oort 1992), which is typically found on the order of 1 K $(1 \text{ day})^{-1}$. In the absence of convective overturning, the diabatic heating term is typically quite small at $10^{-9}\ K\ m^{-1}s^{-1}$. Synoptic-scale wind fields and thermodynamic conditions in weakly baroclinic environments typifying warm season conditions across the central and eastern United States are estimated from observational work, such as Portis and Lamb (1987) for vertical motion, and readily observed horizontal wind and temperature gradients, which were assessed from constant pressure analyses.

Based on the synoptic scaling in Table 1, the *horizontal advection of lapse rate* is 1 to 2 orders of magnitude greater than the other terms. A long downstream transport of the EML plume is plausible when the other terms are small. Although γ is not conserved, synoptic conditions exist that allow horizontal advection of lapse rate to dominate over the other physical processes in (1); these patterns are described through composite and trajectory analysis in Section 4.

The non-advective terms in (1) help explain changes to the EML plume that normally prevent the EML from persisting long enough to reach the NEUS. For instance, a mid-tropospheric diabatic heating maximum (e.g., resulting from latent heat of condensation, *L*, within deep moist convection) would decrease the lapse rate below the maximum having a deleterious effect on the EML plume. One can roughly consider these effects within an area of thunderstorms using a latent heat of condensation term from the 1st law of thermodynamics, *L* dw_s, where w_s is the saturation mixing ratio. Taking *L* as a constant and assuming development of a deep updraft over ~20 minutes yields the following estimate of the diabatic heating term:

$$\frac{\partial \gamma}{\partial t} = \frac{L}{c_p}\frac{\partial}{\partial z}\left(\frac{dw_s}{dt}\right) = \frac{2.5x10^6\ J\ kg^{-1}}{1004\ J\ kg^{-1}K^{-1}}\left(\frac{1}{10^4\ m}\right)\left(-\frac{10^{-2}\ kg/kg}{10^3\ s}\right) = -2.5x10^{-6}\ Km^{-1}s^{-1} \qquad (2)$$

which equates to a decrease in lapse rate of -9 $K\ km^{-1}(hr)^{-1}$. While (2) ignores the counteracting effect of vertical advection of lapse rate, it is clear that deep moist convection quickly eradicates any portion of the EML it processes, likely trending the layer to moist adiabatic. Likewise, whenever differential ageostrophic temperature advection is positive – as would typically occur downstream of an amplifying baroclinic wave, secondary circulation of a jet entrance region, or frontogenetic circulation - lapse rates decrease with time. Since the EML will often become entrained in an increasingly baroclinic environment over time, differential ageostrophic temperature advection can potentially become large and lead to erosion of the EML plume.

The vertical advection and stretching terms are negligible within the EML plume as these terms are numerically small as γ approaches Γ_d. However, at the EML base, the vertical stretching term is important for cap removal during the convective initiation process when vertical velocity increases with height. Conversely, near mid-level anticyclones, subsidence increasing with height at the capping inversion interface contributes to a strengthening of the inversion, which has implications for maintenance of the EML plume over time, as elaborated upon in Section 4.

3. Data and Methodology

a. Severe weather report and sounding databases

The Storm Prediction Center (SPC) severe weather database was systematically searched May 1st through September 30th from 1970-2006 using the SVRPLOT software program (Hart 1993) for reports over New England, New York, New Jersey, Pennsylvania, and small portions of adjacent states (Fig. 3). As shown in Table 2, a total of 30,617 severe weather reports were found (an average of 827 per warm season). Of these, only 929 reports (3%) met SIG SVR criteria over 447 individual event days. Importantly, these 3% account for a majority of the total severe weather fatalities (57.3%) and injuries (61.8%).

For the SIG SVR report days, regional rawinsonde data were utilized to search for the presence of an EML. An "EML sounding" was classified using the following criteria:

1.) An elevated (not surface-based) environmental lapse rate greater than or equal to 8.0 ^{o}C km^{-1} through a depth of 200 mb or greater.

2.) An increase in the environmental relative humidity with height from a relative minimum at the bottom of the layer of steep lapse rate, as defined above, through the depth of the steep lapse rate layer.

The lapse rate criteria were arrived at subjectively, based on an initial inspection of soundings from several candidate cases. While the ultimate choice is arbitrary, we believe marginal or questionable EML events were reasonably eliminated from consideration based on these values. Additionally, the temporal and spatial resolution of the rawinsonde network is such that some subjectivity was necessary in determining if the EML was present at the location of SIG SVR; nearby soundings were often convectively contaminated by 00 UTC. In those cases, lapse rate evolution from available reanalysis datasets (described in Section 3b) were consulted to help determine continuity of the EML into the area of interest.

This procedure yielded 34 SIG SVR event days from 1970-2006 (7.6% of the significant severe event day total) associated with EML soundings, with a total of 189 SIG SVR reports (20.3% of the 929 reports). Significant hail reports were found at a disproportionately high percentage within the EML subset at 35.9%, while significant tornadoes occurred at percentages close to the EML report subtotal at 19.2%. We suspect significant wind reports are underrepresented, since a *measured* gust of ≥65 kts is required (as opposed to "wind damage" reports that might have occurred owing to significant wind).

To add perspective on the importance of the EML cases (including non-quantified significant wind events), the authors tallied all fatalities and injuries due to severe weather of any magnitude on the EML event days (Table 2). Although the EML event day reports accounted for only 0.1% of all severe weather reports in the NEUS, 109 fatalities (52.9% of the total) and 1451

injuries (45% of the total) occurred, placing great importance on accurate forecasts of EML related severe weather events.

In addition to the systematically determined 34 EML event days, the authors utilized a SPC on-line publication concerning historic derechos to discover an additional EML associated event in 1969. Also, we would be remiss not to include the 9 June 1953 Worcester, Massachusetts tornado as part of the dataset because of our a priori knowledge of the case, its destructive impact, and 74 km track. While these 2 earlier events were not part of the systematic detection scheme applied to the 1970-2006 period, associated soundings met required criteria and increased the available sample to 36 events for the composite and trajectory analyses. Tables 3 and 4 give summary descriptions of the EML associated SIG SVR events used in this study.

b. Composites, trajectories, and case studies

Using the National Centers for Environmental Prediction (NCEP) / National Center for Atmospheric Research (NCAR) global reanalysis (Kalnay et al. 1996), we constructed composite analyses of 700mb heights, temperatures, 700-500 mb lapse rates, 4-layer Lifted Index, and sea level pressure and their 1968-1996 climatological anomalies for the 36 EML event days and 413 non-EML SIG SVR days. The composites were created using straight averages on the native geo-referenced grid. Combining events in this way yields a certain degree of spatial smoothing in the composites and is one reason individual case studies are also shown later in the paper. That said, the composite analyses are useful in drawing out common meteorological features across the range of EML related SIG SVR events.

For each SIG SVR event day, the date and time of the first severe weather report was determined. The global reanalysis data is available at 6-hourly sub-synoptic time steps (00, 06, 12, 18 UTC), and the closest time step before the first report for each event was utilized in the

composite (defined as $t = t_o$). Additional composites were generated at 6-hour time increments working backward from the event in time through 5 days (i.e., t_o - 6 h, t_o – 12 h, …, t_o – 120 h).

The National Oceanic and Atmospheric Administration (NOAA) Air Resources Laboratory Hybrid Single-Particle Lagrangian Integrated Trajectory (HYSPLIT) model (Draxler and Hess 1997, 1998) was utilized to produce backward Lagrangian trajectories based upon the global reanalysis dataset for each of the 36 EML events. Backward Lagrangian trajectories were generated at 250 m AGL, and every 1 km from 1-6 km AGL for a duration of 96 hours. A series of low to mid tropospheric trajectories were run to assess airflow characteristics at different levels and also to account for the variability in the EML plume height. The starting point for each generated backward trajectory corresponded to the location (latitude/longitude pair) of the first SIG SVR report, with the starting time rounded to the nearest hour. Lastly, two brief case studies are presented using archival sources of surface and upper air data.

4. Synoptic Composite and Trajectory Analyses

a. Composite analysis

Several salient synoptic signals are apparent in the composite analyses, with distinctions between the EML and non-EML composites. We focus our discussion at 700 mb because it is embedded within the EML. The mean 700-mb heights for the EML composites (Fig. 4a, c, e) reveal a ridge axis extending from the western Atlantic ocean westward across the southeastern and south-central United States, with a northward extension of the ridge into the mid-Mississippi and Tennessee River valleys. The mean ridge is comparatively stronger and displaced northward compared to the non-EML composite (Fig. 4b, d, f), with stronger anticyclonic curvature in the height field downstream of the Rockies in the EML composite at t_o – 48 h (Fig. 4a) and t_o – 24 h

(Fig. 4c). Likewise, a positive geopotential height anomaly builds to near 36 m across the Ohio Valley and Southern Great Lakes region between t_o – 48 h (Fig. 4a) and t_o – 24 h (Fig. 4c) in the EML composite, and then flattens in response to a low-amplitude mean shortwave trough and associated negative height anomalies moving eastward across the Great Lakes at t_o (Fig. 4e). The negative height anomaly over the northern Great Lakes suggests the prevalence of an embedded shortwave trough in the EML events, which is presumably providing the synoptic-scale ascent for cap removal and convective initiation. The northward displacement of the ridge and the approaching trough are important contributors to the relatively strong belt of westerly geostrophic flow that develops in the mean across the NEUS at t_o (Fig. 4e). The temporal evolution of the non-EML mean height and height anomaly composite is different, showing the development of a more highly amplified mean 700 mb trough and stronger negative geopotential height anomaly field (-27 to -30 m) across the upper Mississippi Valley into the Great Lakes Region (Fig. 4d, f) with southwesterly geostrophic flow across the NEUS at t_o (Fig. 4f). The positive height anomaly (of 9 to 15 m) to the south and east is significantly weaker. There also exists a persistent, negative height anomaly (on the order of 10 m) corresponding to a slightly stronger mean West Coast trough axis in the EML composite, which likely aids in the ejection of the EML plume from the Intermountain West; the non-EML composite shows a ridge across the central Rockies.

The advective nature of the EML is evident in the associated temporal evolution of the 700 mb temperature anomaly field. A positive anomaly maxima moves from the Central Plains at t_o – 48 h (Fig. 5a), elongating across the Great Lakes Region at t_o – 24 h (Fig. 5c), and then into the NEUS as it becomes entrained in the strong west-northwest flow downstream of the Great Lakes mean shortwave trough at t_o (Fig. 5e). Temperature anomalies at 700 mb of +3 to

+3.5 ^{o}C exist across New York, Pennsylvania, and far western New England at t_o (Fig. 5e). In the non-EML composite (Fig. 5b, d, f), the zonal positive temperature anomaly with connection back to the Rockies is absent, and the anomaly field is of a lower magnitude (Fig. 5b), on the order of +1 ^{o}C. This is likely the result of synoptic-scale warm advection downstream of the mean trough position, with a similar magnitude negative temperature anomaly upstream of the mean trough axis over the north-central U.S. and south-central Canada at t_o (Fig. 5f). Time series loops showing the evolution of these and additional fields are available on-line [http://weather.ou.edu/~pbanacos/EML/supplement/home.html; Editor – need to host on AMS website prior to press].

Looking specifically at 700 – 500 mb lapse rates, at t_o – 48 h, a plume of steep lapse rates extends from Colorado northeastward across the central Plains into the Upper Mississippi Valley (Fig. 6a). The EML composite mean value of 700 - 500 mb lapse rate is on the order of 7.5 – 8.0 ^{o}C km^{-1}, with anomalies on the order of +1 ^{o}C km^{-1}. At t_o – 24 h (Fig. 6b), the EML plume has elongated and extends eastward across the Great Lakes region. Finally, at t_o (Fig. 6c), the EML plume extends across the southern half of New York, Pennsylvania, and into southern New England. It appears the shortwave trough axis at 700 mb (Fig. 5e) has suppressed the EML plume slightly southward and eastward in the mean at t_o. Consistent with Farrell and Carlson (1989), the occurrence of SIG SVR was frequently on the poleward edge of the EML plume for individual events in the dataset (not shown). The correspondence is good between the positive 700 mb temperature anomaly and the positive lapse rate anomaly. This suggests that the 700 mb thermal ridge axis and associated anomalies can serve as a proxy for the general location of the EML plume and can cue the forecaster to its possible existence.

The sea-level pressure field at t_o is similar in the EML and non-EML composites (Fig. 7), which further points to the relevance of what is occurring aloft in the EML layer. The composite mean best low-level lifted index at t_o (Fig. 7) shows greater potential instability in the EML composite (Fig. 7a).

b. Trajectory analysis

For discussion purposes, our attention is focused on the backward trajectories starting at 3 km AGL, which generally corresponded to the lower to middle portion of the EML. While individual trajectories exhibit a large variance, it is apparent that many of the 36 trajectories exhibit neutral to anticyclonic curvature across the Plains and Midwest (Fig. 8a), consistent with the anomalously strong mean 700 mb ridge over the Tennessee Valley. None of the trajectories approach from the south; most originate or cross the Intermountain West, consistent with the paths of the 700 mb temperature anomaly and 700-500-mb lapse rate composites.

Interestingly, backward trajectories in 10 of the 36 events exhibited at least a three-fourths anticyclonic loop enroute to the SIG SVR starting location. This subset of events is shown separately in Fig. 8b. Some of these events originate east of the Front Range, though it is noteworthy that backward trajectories from 4 km and 5 km AGL often originated from the Intermountain West. Of the 10 events, 9 were associated with subsidence (descending air parcel trajectories) in the period 12-36 hours prior to the event (not shown).

A 3-km AGL backward trajectory time-height analysis was developed from the 36 individual EML events (Fig. 9). After t_o -51 h, the mean trajectory (top line) begins subsiding, persisting until roughly 14 h before the event. Mean instantaneous vertical motion (bottom line) is about 1 μb s^{-1}, consistent with the magnitude of synoptic-scale vertical velocities. Fourteen hours before the first significant severe report, the mean instantaneous vertical velocity reverses

sign showing ascent, and reaches roughly -1 μb s^{-1} at t_o -3 h. The box-and-whisker analysis of 6-h pressure change following trajectory motion, $\left.\frac{Dp}{Dt}\right|_{6h}$, shows consistency in this pattern for the majority of trajectory members, revealing persistent subsidence 1 to 2 days prior to the event, followed by ascent as trajectories approach the time and location of the first SIG SVR report. The period of ascent is short in duration, but almost certain near t_o.

Consistent with the lapse rate tendency equation (1), mean subsidence from t_o-51 to t_o-14 h likely strengthens the capping inversion at the base of the EML (through differential downward vertical motion, in Term 5 of (1)). A strong cap and large-scale subsidence would generally not be conducive for widespread deep moist convection, which would otherwise have a deleterious impact on the EML plume. Thereafter, the rising motion in the hours prior to the first SIG SVR report is consistent with lift necessary for weakening the cap and a necessary ingredient for deep moist convection (Doswell 1987). There is also consistency between the time series of vertical motion and the composite analyses. In the composite 700 mb analysis, there existed anticyclonic curvature in the flow, contributing to downward motion east of the Rockies, until such time that the parcel is entrained in a rising air stream in advance of the mean shortwave trough translating eastward across the Great Lakes region.

Given the paucity of EML significant severe weather episodes over the NEUS, we hypothesize that both horizontal advection *and* downward vertical motion within the EML plume are essential factors for EML maintenance and transport over large distances. Furthermore, the timing of large-scale ascent is important in lessening convective inhibition and ultimately in the release of the instability over the NEUS. Mesoscale features might also be expected to play an important role, but were beyond the scope of this research.

5. Case Studies

a. Eastern New York/Western Massachusetts tornadoes; 28 Aug 1973

On 28 August 1973, three significant tornadoes occurred in Eastern New York and Western Massachusetts with a supercell thunderstorm that developed in the Adirondack Mountains of New York. The storm tracked south-southeastward producing a near-continuous 350 km swath of severe weather before weakening over Long Island Sound. An F4 tornado was responsible for 3 deaths and 36 injuries when it struck a truck stop in West Stockbridge, MA around 1740 UTC, with an additional fatality at a nearby house. At least two other severe thunderstorms affected eastern New England with large hail, damaging winds, and isolated tornadoes.

At 28/12 UTC, a 700 mb anticyclone was centered over Southeastern Ohio with a ridge axis extending northward across eastern Ontario. A plume of 700-500 mb lapse rates of 8 ^{o}C km^{-1} or greater was present in an arc from Colorado northeastward to Southwestern Ontario, and then southeastward into the Ohio Valley (Fig. 10). A 96-hour backward trajectory analysis (Fig. 11) revealed that the EML likely originated over the Mexican Plateau and was advected northeastward around the mid-tropospheric ridge, finally turning southeastward over the Great Lakes before reaching ALB at 28/12 UTC. The progression of the EML plume is evident in observed soundings analyzed at 24 h intervals (Fig. 12a-d) near the trajectory. Note that the plume exhibited minimal change in character despite being advected nearly 3500 km, as evidenced by the nearly dry adiabatic lapse rates in the 800-500 mb layer on the 28/12 UTC Albany, NY (ALB) sounding (Fig. 12d). The steepest lapse rates do not necessarily conform to common fixed layers (e.g., 700-500 mb), highlighting the importance of examining soundings.

Fig. 13a-d shows the chronological progression of the EML plume via the 700 mb temperature anomaly maximum as it "breaks off" from the source region of the High Plains of Texas and elevated terrain of New Mexico and is advected into the NEUS over 96 h. At 28/12 UTC (Fig. 13d), the 700 mb temperature anomaly maximum shifted southward into the Mid Atlantic States as a thermal trough over Quebec embedded in mid-tropospheric northwest flow translated southeastward. The shortwave trough was likely responsible for providing the necessary ascent for cap removal and initiation of deep moist convection. Note also that the convection occurred on the northern fringe of the EML, as has been found in similar events (e.g., Farrell and Carlson 1989).

The 28/12 UTC ALB sounding was modified using the 28/20 UTC surface temperature of 31 ^{o}C and dewpoint of 21 ^{o}C, to better approximate the thermodynamic environment close to the occurrence of the F4 tornado (Fig. 14). The 900-700 mb layer was modified slightly to account for assumptive cooling aided by ascent associated with the approaching 700 mb thermal trough shown in Fig. 13d. The modified sounding revealed a potentially unstable environment with 100 mb mean-mixed CAPE (CIN) of approximately 2750 (-60) J/kg. The strong instability combined with northwesterly surface - 6 km vertical shear values of around 25 ms^{-1} and weak low-level linear forcing allowed for long-lived, isolated supercells.

b. Northern New England and Southern Quebec Derecho; 5 July 1999

A significant nocturnal derecho affected far northern New England and southern Quebec during the early morning hours of 5 July 1999 resulting in two fatalities, several injuries, as well as considerable destruction of property and forest (Mainville 1999). The derecho began as a cluster of thunderstorms over North Dakota early on 4 July 1999 and subsequently grew upscale

while traveling over 2000 km, finally weakening over coastal Maine early in the morning on 5 July 1999 (Fig. 15).

The 05/00 UTC rawinsonde plot at 700 mb revealed a strong mid tropospheric anticyclone centered over Kentucky along with anomalously warm temperatures (+13ºC to +15ºC) as far north as southern Ontario and Quebec (Fig. 16). A nearly continuous plume of anomalously steep mid tropospheric lapse rates extended from the NEUS westward to the Intermountain West. The mid-tropospheric trajectory suggests the source region of the EML was the Southwest U.S., and the EML was then advected northeastward over a period of 96 hours (Fig. 17). Observed soundings were again examined at 24-hour intervals near the trajectory to verify the presence of the EML (Fig. 18 a-d). The 05/00 UTC rawinsonde at Maniwaki, Quebec (Fig. 18d) confirmed the presence of an EML in the region with near-dry adiabatic lapse rates and increasing relative humidity with height in the 700-500 mb layer. This rawinsonde conveniently serves as a "near-proximity" sounding, as the derecho passed over the site approximately 5 h after the rawinsonde was launched. The presence of the EML and the associated capping inversion allowed for an unusual buildup of boundary layer moisture (surface dewpoints near 23-24 ^{o}C with surface theta-e values in excess of 350 K) which in turn aided in unusually strong instability prior to the passage of the derecho. The combination of 45 kts of surface to 6 km shear and surface-based CAPE values near 3500 J kg^{-1} allowed for the maintenance of the derecho as it entered Quebec and northernmost New England. Once the mesoscale convective system became organized, strong low-level ascent along the leading edge of the existing cold pool allowed parcels to reach the level of free convection, within a deep, unidirectional flow regime strongly favoring forward propagation (Corfidi 2003). Organized convection would not ordinarily be expected in an area with 700 mb temperatures in excess of

13˚C (owing to a strong cap). However, a subtle shortwave trough embedded in the mid tropospheric northwest flow (not shown) likely provided sufficient ascent and resultant cooling within the inversion layer to sustain incipient deep convection. The 05/12 UTC Maniwaki sounding (not shown) indicated an observed 700 mb temperature of +8.4˚C, 5.2˚C cooler than the observed 700 mb temperature just 12 h earlier. The advection of the EML plume is also evident in 700 mb temperature anomalies of +2 to +3 standard deviations denoting the location of the EML plume as it moved around the northern periphery of the mid-level ridge (Fig. 19 a-d).

6. Summary and Future Work

a. Summary

The authors catalogued warm season SIG SVR reports in the NEUS from 1970-2006. Events were categorized as either being associated with or not-associated with EML air based on examination of regional soundings. The 7.6% of SIG SVR event days associated with an EML disproportionately accounted for 52.9% of the fatalities and 45% of the injuries over the study period and comprised historically important severe weather events in the region.

A lapse rate tendency equation and scale analysis revealed horizontal advection as a plausible means of long downstream transport of EML air from the Intermountain West into the NEUS, with large-scale subsidence maintaining the EML plume and capping inversion en route. A sample of 36 EML events allowed for composite and trajectory analysis and revealed several key synoptic findings: (1) a mean 700mb anticyclone centered over the Tennessee River Valley, north and west of its normal location, (2) a 700mb trough along the West Coast that results in ejection of the EML plume northeastward across the Great Plains, (3) anticyclonic flow (or complete trajectory “loops” in some cases) across the Plains and upper Mississippi Valley,

yielding mean downward motion and limited convection, maintaining the EML plume until it moves downstream of the ridge axis, and (4) a shortwave trough embedded in enhanced and moderately strong west to northwest mid-level flow north of the ridge position across the Great Lakes, which ultimately entrains the EML air and contributes to upward motion and convective initiation for the events in the NEUS. When compared, the EML and non-EML composites deviated significantly from each other, with the former revealing a west to northwest mid-level flow regime, and a stronger 700 mb positive temperature anomaly of +3 to +4 ^{o}C owing to the presence of the EML itself. Synoptic case studies were employed to further elucidate the key findings listed above, consistent with how an operational forecaster would see an individual EML event unfold in sounding, upper air, and departure from climatology datasets.

There are two main limitations to this study. First, the methodology precluded an examination of null cases; i.e., scenarios that could bring an EML plume across the study area but do not result in SIG SVR. A lack of forcing for ascent or dry, cool boundary layer conditions yielding insufficient CAPE could allow EML air to pass the region without development of deep moist convection. Secondly, it is important to note that the EML alone does not determine storm mode; the events in this study include historical derecho and tornadic supercell events. However, both modes pose risk to life and property, and one is not necessarily of greater severity than the other. Factors such as the magnitude of vertical shear, mesoscale boundaries, and the geometry of upward motion would also need to be considered to determine storm mode.

b. Future work

We foresee opportunities to pursue this topic further. Most interesting would be a model-based study geared to quantitatively assess each term of the lapse rate tendency equation in various situations *to better understand how the EML evolves over time across the central and*

eastern United States. Examination of convective mode in EML environs and null cases would also be topics worthy of future investigations; one could start from the sounding or reanalysis data to systematically catalog all steep lapse rate occurrences as a means of finding null events. Lastly, construction of maximum layer lapse rate maps (e.g., 100 or 200 mb deep) above the boundary layer not arbitrarily linked to specific pressure levels (e.g., 700-500 mb) would likely show potential EMLs and their boundaries more vividly for forecasters, and such procedures would be a worthwhile incorporation into graphical workstations.

Acknowledgments. This project stemmed from enlightening early discussions with Jon Finch (NWS DDC) and Bob Johns (SPC), and we are grateful for their insights. Drs. John Gyakum and Eyad Atallah (McGill Univ.) created the lapse rate composites used in Fig. 6 and Bob Johns provided the derecho isocrone analysis used in Fig. 15. The NCAR/NCEP global reanalysis images were provided by the NOAA/ESRL Physical Sciences Division from their Web site at http://www.cdc.noaa.gov/. The NOAA Air Resources Laboratory (ARL) READY website (http://www.arl.noaa.gov/ready.html) was used for the HYSPLIT trajectories. The paper benefited from reviews by Steve Corfidi, Joe Dellicarpini, Walter Drag, Jim Hayes, Andy Nash, Dave Radell, Dave Schultz, Jay Shafer, Paul Sisson, Bob Thompson, and Jeff Waldstreicher. We also thank the three anonymous reviewers for helping to improve the manuscript.

APPENDIX

Lapse Rate Tendency Equation

The lapse rate tendency equation described in Section 2 is derived below. Variations of the lapse rate tendency equation derivation below also appear elsewhere (e.g., Air Weather Service 1990, Doswell 1997, class notes).

The environmental lapse rate, γ, is defined as:

$$\gamma = -\frac{\partial T}{\partial z} \tag{A1}$$

where T is temperature and z is geometric height. The lapse rate tendency, expressed as $\frac{\partial \gamma}{\partial t}$, represents the local time rate of change of environmental lapse rate. Starting from the 1st law of thermodynamics:

$$dh = c_p dT - \alpha dp \tag{A2}$$

where dh is the inexact differential denoting an infinitesimal change in heat, α is the specific volume, or the inverse of density (i.e., $1/\rho$), c_p is the specific heat of air at constant pressure, and p is pressure. Dividing both sides of the equation by the inexact differential dt, expanding the total derivative dT/dt, and substitution with the hydrostatic equation ($dp = -\frac{g dz}{\alpha}$) yields:

$$\frac{dh}{dt} = c_p \left[\frac{\partial T}{\partial t} + \mathbf{V} \cdot \nabla_h T + w \frac{\partial T}{\partial z} \right] + g \frac{dz}{dt} \tag{A3}$$

We will define the diabatic heating as, $\frac{dh}{dt} \equiv Q$. Also note that $\frac{dz}{dt}$ is the vertical velocity w.

Next, we differentiate with respect to height, $\frac{\partial}{\partial z}$, and multiply both sides by -1:

$$-\frac{\partial Q}{\partial z} = c_p \left[\frac{\partial}{\partial t}\left(-\frac{\partial T}{\partial z} \right) + \mathbf{V} \cdot \nabla_h \left(-\frac{\partial T}{\partial z} \right) + w \frac{\partial}{\partial z}\left(-\frac{\partial T}{\partial z} \right) - \frac{\partial \mathbf{V}}{\partial z} \cdot \nabla_h T - \frac{\partial w}{\partial z}\frac{\partial T}{\partial z} \right] - g \frac{\partial w}{\partial z} \tag{A4}$$

Then by substitution with (A1), and noting that $\frac{g}{c_p} = \Gamma_d$, where Γ_d is the dry adiabatic lapse rate, the following equation is achieved:

$$-\frac{\partial Q}{\partial z} = c_p \left[\frac{\partial \gamma}{\partial t} + \mathbf{V} \cdot \nabla_h \gamma + w \frac{\partial \gamma}{\partial z} - \frac{\partial \mathbf{V}}{\partial z} \cdot \nabla_h T - \frac{\partial w}{\partial z}\left(\Gamma_d - \gamma \right) \right] \tag{A5}$$

Rearrangement of terms to solve for the local change in lapse rate, $\frac{\partial \gamma}{\partial t}$, yields a lapse rate tendency equation, which is described in Section 2:

$$\frac{\partial \gamma}{\partial t} = -\frac{1}{c_p}\frac{\partial Q}{\partial z} - \mathbf{V} \cdot \nabla_h \gamma - w\frac{\partial \gamma}{\partial z} + \frac{\partial \mathbf{V}}{\partial z} \cdot \nabla_h T + \frac{\partial w}{\partial z}\left(\Gamma_d - \gamma\right) \tag{A6}$$

REFERENCES

Air Weather Service, Revised March 1990: *The Use of the Skew-T/Log-P Diagram in Analysis and Forecasting*, AWS/TR-79/006, 153 pp.

Carlson, T. N., and F. H. Ludlam, 1968: Conditions for the occurrence of severe local storms. *Tellus*, **20**, 203-226.

_____, S. G. Benjamin, G. S. Forbes, and Y. F. Li, 1983: Elevated mixed layers in the regional severe storm environment: Conceptual model and case studies. *Mon. Wea. Rev.*, **111**, 1453-1473.

Concannon, P.R, H.E. Brooks, and C.A. Doswell III, 2000: Climatological risk of strong and violent tornadoes in the United States. Preprints*, 2nd Conf. on Environmental Application.* Long Beach, CA, Amer. Meteor. Soc., 212-219.

Corfidi, S. F., 2003: Cold pools and MCS propagation: Forecasting the motion of downwind-developing MCSs. *Wea. Forecasting*, **18**, 997-1017.

Doswell, C. A., 1987: The distinction between large-scale and mesoscale contribution to severe convection: A case study example. *Wea. Forecasting*, **2**, 3 – 16.

_____, and L. F. Bosart, 2001: Extratropical synoptic-scale processes and severe convection. *Severe Convective Storms*, C. Doswell, Ed., Amer. Meteor. Soc., 27-69.

_____, H. E. Brooks, and M. P. Kay, 2005: Climatological estimates of daily local nontornadic severe thunderstorm probability for the United States. *Wea. Forecasting*, **20**, 577-595.

Draxler R. R., and G. D. Hess, 1997: Description of the HYSPLIT_4 modeling system. NOAA Tech. Memo. ERL ARL-224, 24 pp.

_____, and G. D. Hess, 1998: An overview of the HYSPLIT_4 modelling system for trajectories, dispersion, and deposition. *Aust. Meteor. Mag.*, **47**, 295–308.

Farrell, R. J., and T. N. Carlson, 1989: Evidence for the role of the lid and underunning in an outbreak of tornadic thunderstorms. *Mon. Wea. Rev.*, **117**, 857-871.

Fawbush, E. J., and R. C. Miller, 1954: The types of air masses in which North American tornadoes form. *Bull. Amer. Meteor. Soc.*, **35**, 154-165.

Hart, J. A., 1993: SVRPLOT: A new method of accessing and manipulating the NSSFC severe weather data base. Preprints, *17th Conf. on Severe Local Storms*, St. Louis, MO, Amer. Meteor. Soc., 40–41.

Johns R. H., and R. A. Dorr, 1996: Some meteorological aspects of strong and violent tornado episodes in New England and eastern New York. Natl. Wea. Dig., 20(4), 2–12.

Kalnay, E. and Coauthors, 1996: The NCEP/NCAR Reanalysis 40-year Project. *Bull. Amer. Meteor. Soc.*, **77**, 437-471.

Lanicci, J. M., and T. T. Warner, 1991: A synoptic climatology of the elevated mixed-layer inversion over the southern Great Plains in Spring. Part III: Relationship to severe-storms climatology. *Wea. Forecasting*, **6**, 198-213.

_____, and T. T. Warner, 1997: A case study of lid evolution using analyses of observational data and a numerical model simulation. *Wea. Forecasting*, **12**, 228-252.

Mainville, S., 1999: The derecho of 4-5 July 1999 in southern Quebec. Technical Note, Quebec Region, **99N-04**, Environment Canada.

Peixoto, J. P., and A. H. Oort, 1992: *Physics of Climate*. American Institute of Physics, 520 pp.

Portis, D. H., and P. J. Lamb, 1988: Estimation of large-scale vertical motion over the central United States for summer. *Mon. Wea. Rev.*, **116**, 622-635.

Table List

TABLE 1. Estimation of variables and terms in the lapse rate tendency equation, based on synoptic scale analysis described in Section 2.

TABLE 2. Severe weather and significant severe weather (SIG SVR) reports across the New England states, New York, Pennsylvania, New Jersey, and small portions of adjacent states for the period 1970-2006. SIG SVR percentages are relative to all severe weather reports. EML SIG SVR percentages are relative to all severe weather reports (first value) and significant severe weather reports (second value). EML SIG SVR fatality and injury information is due to all severe weather during the episode (SIG SVR and non-SIG SVR). In the SIG SVR category, fatality and injury information is attributed to significant severe weather reports only.

TABLE 3. EML associated significant severe weather events over the Northeastern United States (1970-2006, plus 2 earlier events). SIG SVR reports refer to the number of significant severe reports available in *Storm Data* (N/A means official reports not available). The Fatal/Injury column references the total number of weather related fatalities and injuries associated with the event, respectively. EML soundings refer to soundings meeting EML criteria preceding the event. Mid-level flow refers to mean wind direction in the mid-troposphere during the event.

TABLE 4. Written excerpts from *Storm Data* for several EML events.

Tables

TABLE 1. Estimation of variables and terms in the lapse rate tendency equation, based on synoptic scale analysis described in Section 2.

$\lvert\nabla\gamma\rvert \sim 10^{-8}\,K\,m^{-2}$	$w \sim 10^{-2}\,m\,s^{-1}$	$\frac{1}{c_p}\frac{\partial Q}{\partial z} \sim 10^{-9}\,K\,m^{-1}s^{-1}$
$\frac{\partial\gamma}{\partial z} \sim 10^{-6}\,K\,m^{-2}$	$\left\lvert\frac{\partial \mathbf{V}_a}{\partial z}\right\rvert \sim 10^{-3}\,s^{-1}$	$\lvert\nabla T\rvert \sim 10^{-5}\,K\,m^{-1}$
$(\Gamma d - \gamma) \sim 10^{-3}\,K\,m^{-1}$	$\lvert\mathbf{V}\rvert \sim 10\,m\,s^{-1}$	$\frac{\partial w}{\partial z} \sim 10^{-6}\,s^{-1}$

Term *a*: $\frac{1}{c_p}\frac{\partial Q}{\partial z} \sim 10^{-9}\,K\,m^{-1}s^{-1}$

Term *b*: $\mathbf{V}\cdot\nabla\gamma \sim 10^{-7}\,K\,m^{-1}s^{-1}$

Term *c*: $w\frac{\partial\gamma}{\partial z} \sim 10^{-8}\,K\,m^{-1}s^{-1}$

Term *d*: $\frac{\partial \mathbf{V}}{\partial z}\cdot\nabla T \sim 10^{-8}\,K\,m^{-1}s^{-1}$

Term *e*: $\frac{\partial w}{\partial z}(\Gamma_d - \gamma) \sim 10^{-9}\,K m^{-1}s^{-1}$

TABLE 2. Severe weather and significant severe weather (SIG SVR) reports across the New England states, New York, Pennsylvania, New Jersey, and small portions of adjacent states for the period 1970-2006. SIG SVR percentages are relative to all severe weather reports. EML SIG SVR percentages are relative to all severe weather reports (first value) and significant severe weather reports (second value). EML SIG SVR fatality and injury information is due to all severe weather during the episode (SIG SVR and non-SIG SVR). In the SIG SVR category, fatality and injury information is attributed to significant severe weather reports only.

	All SVR	SIG SVR	EML SIG SVR Subset
Event Days	N/A	447	34* (7.6%)
Reports	30,617	929 (3.0%)	189 (0.1%, 20.3%)
Reports/event day	N/A	2.1	5.6
Wind	22,931	473 (2.1%)	69 (<0.1%, 14.6%)
Tornado	1,283	261 (20.3%)	50 (3.9%, 19.2%)
Hail	6,403	195 (3.0%)	70 (1.1%, 35.9%)
Fatalities	206	118 (57.3%)	109# (52.9%)
Injuries	3228	1995 (61.8%)	1451# (45.0%)

* Does not include 9 June 1953 and 4 July 1969 events used in composite analyses.

Includes all fatalities and injuries from all severe reports on 34 EML event days.

TABLE 3. EML associated significant severe weather events over the Northeastern United States (1970-2006, plus 2 earlier events). SIG SVR reports refer to the number of significant severe reports available in *Storm Data* (N/A means official reports not available). The Fatal/Injury column references the total number of weather related fatalities and injuries associated with the event, respectively. EML soundings refer to soundings meeting EML criteria preceding the event. Mid-level flow refers to mean wind direction in the mid-troposphere during the event.

Date	SIG SVR Reports	Fatal/Injury	EML Sounding IDs	Mid-level Flow	Event Comments
09 Jun 1953	3	94/1288	NY9	W	F4 Worcester, MA tornado
04 Jul 1969	N/A	0/0	DAY GRB	NW	Western PA derecho
28 Aug 1973	5	4/37	ALB BUF IAD PIT	NW	F4 West Stockbridge, MA tornado
31 Aug 1973	4	0/0	IAD JFK PIT	NW	F2 tornado in CT
04 Jul 1974	1	0/0	ALB	NW	2.00 in hail in VT
11 Jul 1976	6	2/24	FNT HTS	NW	F3 tornado in PA
10 Jul 1978	1	0/0	DAY SLO	NW	2.00 in hail in PA
05 Jul 1980	1	0/0	DAY HTS SLO	WNW	F2 tornado in western PA
08 Jul 1980	1	0/0	DAY FNT SLO	NW	4.00 in hail in PA
31 May 1985	29	75/851	DAY SLO	W	F4-F5 PA tornado outbreak
24 Jun 1985	12	0/1	WAL	NW	Multiple 2.75in hail in PA
09 Jul 1985	2	0/0	BUF DAY HTS PIT	NW	Multiple 2.00in hail in PA
28 Aug 1988	3	1/3	ALB	WSW	F2 tornado in PA; 2.5 in hail and 70 mph gust in VT
10 Jul 1989	12	1/153	FNT IAD PIT	NW	F4 tornado in CT
30 May 1991	1	0/0	ALB FNT	NW	2.75 in hail in NY
28 Jun 1991	2	0/0	PWM	NW	2.75 in hail in ME
07 Jul 1991	2	0/14	DAY FNT HTS	WNW	Southern Great Lakes

					derecho
10 Jul 1993	2	0/26	ACY PIT	WNW	79 mph gust in NY; 2.00 in hail in CT
29 May 1995	6	3/30	GYX OKX	WSW	F4 Great Barrington tornado
19 Jun 1995	1	0/0	BUF GYX WMW	NW	3.00 in hail in ME
20 Jun 1995	6	0/0	ALB BUF WMW	NW	2.75 in hail in CT
13 Jul 1995	1	0/0	DAY DTX	NW	derecho across OH/ western PA
15 Jul 1995	5	5/11	BUF LWX OKX PIT	NW	Adirondacks derecho
15 Aug 1996	1	0/0	BUF PIT	SW	2.75 in hail in PA
18 Aug 1996	1	0/0	GYX	NW	2.00 in hail in ME
31 May 1998	27	4/132	LWX PIT	W	F3 Mechanicville tornado
24 Aug 1998	2	0/0	ALB OKX	W	2.75 in hail in NH
07 Sep 1998	12	6/79	BUF OKX	WNW	Labor Day derecho
07 Jun 1999	2	0/2	BUF OKX	W	90 mph gust in NY
05 Jul 1999	6	1/5	WMW YQI	WNW	Canadian and northern New England derecho
06 Jul 1999	10	4/4	PIT WAL	W	100 mph gust in NY; 2.75 in hail in MA
20 Jun 2001	5	0/0	ALB GYX	W	2.75 in hail in NY
31 May 2002	6	1/64	CHH LWX	NW	sig wind and sig hail
24 May 2004	5	0/1	LWX PIT	WNW	90 mph gust and 3 in hail in NY
22 Jul 2005	1	0/0	OKX	NW	2 in hail in VT
18 Jul 2006	8	2/14	ALB CHH OKX	W	2.75 in hail in ME; 75 mph gust in PA

Total fatalities/injuries: 203/2739

TABLE 4. Written excerpts from *Storm Data* for several EML events.

Date	Event	Description
10 Jul 1989	F4 Tornado	This major tornado…touched down in Hamden, CT. As many as 350 homes and over 40 businesses were destroyed, resulting in many hundreds of people being displaced. Damage estimates in Hamden alone exceeded 100 million dollars.
28 Jun 1991	Giant Hail	Extensive damage was reported in Calais, ME at (23 UTC) when tennis ball to baseball size hail fell. Cars were dented by the hail and their windows blown out. A car dealership had 55 cars damaged with damage estimated at $135,000. Total damage to cars and homes in Calais was estimated at several hundred thousand dollars.
20 Jun 1995	Giant Hail	Baseball-size hail lasted for up to 20 minutes in Deep River, CT causing hundreds of thousands of dollars in damage. The hailstones broke hundreds of windows in buildings and automobiles, tore holes in roofs, dented siding and automobiles, and ruined gardens. Some automobiles were totaled.
15 Jul 1995	Derecho	One of the most devastating severe weather outbreaks to hit eastern New York… occurred on the morning of July 15$^{th.}$ Extensive tree damage occurred across the area with the Adirondacks being the hardest hit. Damage estimates…indicated that some 900,000 acres of forest were damaged with 125,000 acres of timber in the Adirondack Park sustaining moderate to severe damage. The timber damage (was) estimated at 1 billion board feet with an estimated value of $204 million. Five deaths and eleven injuries occurred with this event.

Figure Captions

FIGURE 1. Juxtaposed rawinsonde data on Skew-T/Log-P diagram from Dodge City, KS (DDC, black) and Albuquerque, NM (ABQ, gray) at 00 UTC 07 June 1990. Wind barbs represent 10 kt (5ms^{-1}) and half barbs represent 5 kt (2.5 ms^{-1}). Surface pressure is denoted for each site. The EML depth on the DDC sounding is depicted, and "CAP" refers to the warmest point within the capping inversion on the DDC sounding. A representative dry adiabat is labeled by Γ_d.

FIGURE 2. Illustration of the effect of physical processes on the local time rate of change of environmental lapse rate, γ. In (a), owing to a diabatic heating maximum, (b) due to horizontal lapse rate advection, (c) due to the vertical advection of lapse rate, (d) due to differential ageostrophic temperature advection, and (e) due to vertical stretching. The sense of the lapse rate tendency is shown at point locations.

FIGURE 3. Plot of all significant severe weather reports over the Northeastern United States from May 1st through September 30th, 1970-2006. Dots and lines represent F2 or greater tornadoes, crosses represent measured convective wind gusts of 65 kts or greater, and circles show hail of 2 inches in diameter or greater.

FIGURE 4. Composite analyses of the mean 700 mb geopotential height (solid contours) and 700 mb height anomaly (shaded) (versus 1968-1996 climatology) based on the NCEP/NCAR reanalysis dataset for all EML events (left column) and all SIG SVR non-EML events (right column). Time t_o corresponds to the 6-hourly sub-synoptic time step preceding the first significant severe weather report for each of n events listed. Composite panels a-b are valid at t_o

– 48 h, panels c-d at t_o – 24 h, and panels e-f at t_o. The contour interval is 15 m and 3 m for the mean geopotential height and height anomaly analyses, respectively.

FIGURE 5. Composite analysis as in Fig. 4, except for 700mb temperature anomaly (shaded, 0.5 ^{o}C shading interval).

FIGURE 6. Composite 700-500mb mean lapse rate for all 36 EML events based on NCEP/NCAR Global Reanalysis data for (a) t_o – 48 h, (b) t_o – 24 h, and (c) at t_o. Solid lines represent γ with a contour interval of 0.5 ^{o}C km^{-1}. Shading represents 700-500mb lapse rate anomaly in tenths of degrees ^{o}C km^{-1} based on 1971-2000 climatological values. Contour interval for the lapse rate anomaly is 0.2 ^{o}C km^{-1}.

FIGURE 7. Composite mean 4-layer best lifted index (Celsius, shaded every 0.5 ^{o}C) and sea-level pressure (solid, isobars every 2 mb) for (a) EML events and (b) non-EML events. Time t_o corresponds to the 6-hourly sub-synoptic time step preceding the first significant severe weather report for each of *n* events listed.

FIGURE 8. Backward 3-km AGL trajectories taken from the location of the first significant severe weather report (marked by circles) rounded to the nearest hour for (a) each of the 36 EML events, and (b) subset of ten trajectories exhibiting three-quarter or greater anticyclonic loops along their path. Each trajectory duration is 96 hours.

FIGURE 9. Time series analysis of 3-km AGL backward trajectories for the 36 EML events. Box-and-whisker graph shows 6-h pressure change following trajectory motion ($\left.\frac{Dp}{Dt}\right|_{6h}$, in mb) with scale on outside of left ordinate. Median pressure change is shown by black line within the box, the box encompasses 25th to 75th percentile pressure change, and ends of whiskers correspond to 10th and 90th percentile pressure change. Lines show time-height cross-section of mean backward trajectory pressure (mb, top line with scale on inside of left ordinate), and mean instantaneous vertical velocity (bottom line, scale on right ordinate). Time along abscissa corresponds to the number of hours before the first significant report. Results are from NOAA HYSPLIT model run on Global Reanalysis dataset.

FIGURE 10. The 700 mb rawinsonde plot at 12 UTC 28 August 1973. Each full (half) barb is 5 ms^{-1} (2.5 ms^{-1}). The 700-500 mb mean lapse rate (^{o}C/km, solid lines every 0.5 degrees) is contoured.

FIGURE 11. The HYSPLIT model 96-hour backward trajectory analysis (plotted every 12 hours) starting at Albany, NY at 12 UTC 28 August 1973. Trajectory 1 approximates the path of the EML plume in the middle troposphere, with time-height analysis shown in bottom panel. Trajectory 2 represents the path of the 2-m (surface) air parcel. Points a-d represent the rawinsonde locations utilized in Fig. 12.

FIGURE 12. Soundings taken at points a through d along "Trajectory 1" in Fig. 11. The soundings are: (a) El Paso, TX 00 UTC 25 Aug 1973, (b) North Platte, NE 12 UTC 26 Aug

1973, (c) Sault Saint Marie, MI 12 UTC 27 Aug 1973, and (d) Albany, NY 12 UTC 28 Aug 1973.

FIGURE 13. The 700 mb temperatures (^{o}C, solid contours) and anomalies (standard deviations from the 1961-90 climatological mean, shaded) derived from the NCEP/NCAR reanalysis at (a) 12 UTC 25 Aug 1973; (b) 12 UTC 26 Aug 1973; (c) 12 UTC 27 Aug 1973; (d) 12 UTC 28 Aug 1973.

FIGURE 14. The 28/12 UTC ALB sounding modified for 28/20 UTC temperature and dewpoint from the surface observation at ALB. Mixed layer CAPE and CIN are shaded.

FIGURE 15. Area affected by the 4-5 July 1999 derecho (scalloped line) with isocrones of the leading edge gust front at 3-h intervals (curved lines). Crosses indicate locations of wind damage or estimated wind gusts above severe limits (25 ms^{-1} or higher). (Analysis provided by Bob Johns)

FIGURE 16. As in Fig. 10 except at 00 UTC 5 Jul 1999.

FIGURE 17. As in Fig. 11 except starting from Maniwaki, Quebec at 00 UTC 05 Jul 1999. Points a through d represent the rawinsonde locations shown in Fig. 18.

FIGURE 18. Observed soundings along Trajectory 1 in Fig. 17 at (a) Desert Rock, NV 00 UTC 02 Jul 1999; (b) Grand Junction, CO 00 UTC 03 Jul 1999; (c) Aberdeen, SD 00 UTC 04 Jul 1999; (d) Maniwaki, Quebec 00 UTC 05 Jul 1999.

FIGURE 19. As in Fig.13 except at (a) 06 UTC 2 Jul 1999; (b) 06 UTC 3 Jul 1999; (c) 06 UTC 4 Jul 1999; (d) 06 UTC 5 Jul 1999.

Figures

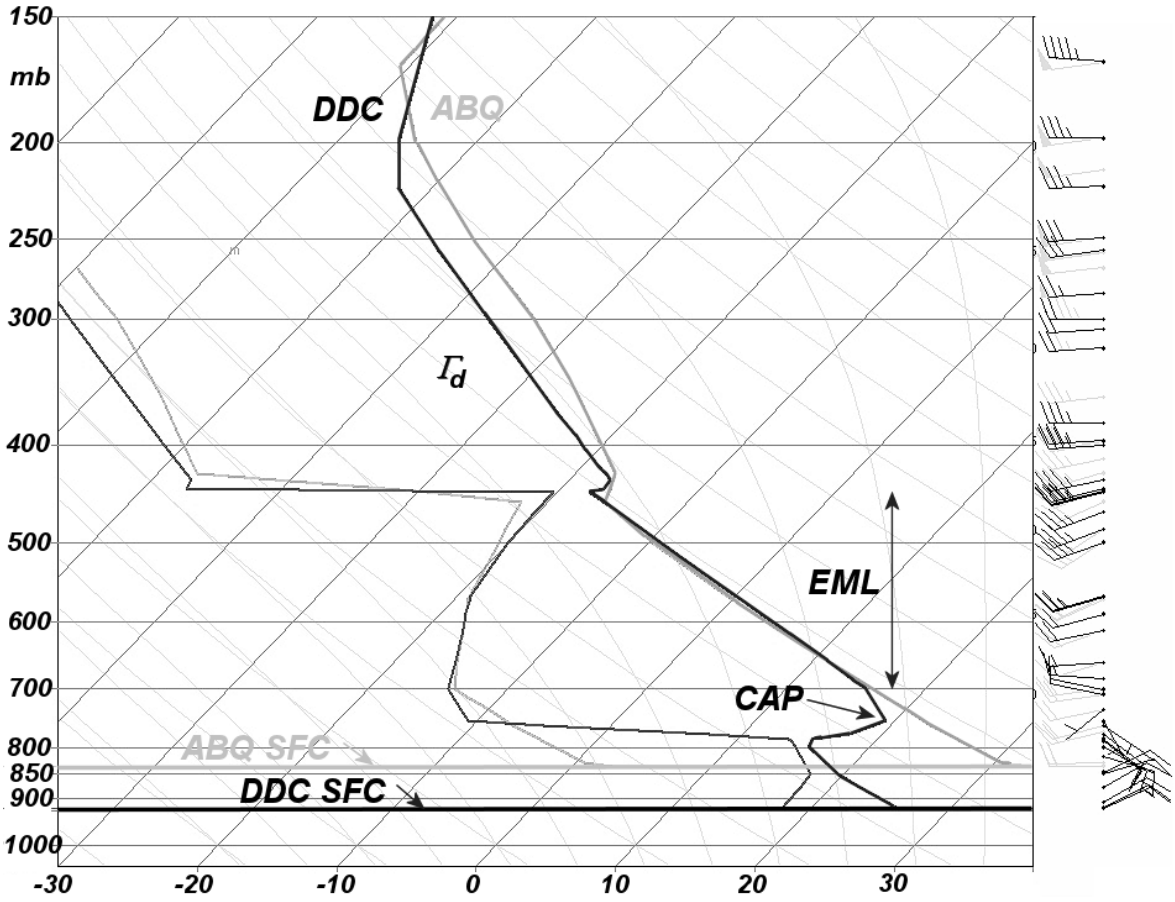

FIGURE 1. Juxtaposed rawinsonde data on Skew-T/Log-P diagram from Dodge City, KS (DDC, black) and Albuquerque, NM (ABQ, gray) at 00 UTC 07 June 1990. Wind barbs represent 10 kt ($5 ms^{-1}$) and half barbs represent 5 kt ($2.5 ms^{-1}$). Surface pressure is denoted for each site. The EML depth on the DDC sounding is depicted, and "CAP" refers to the warmest point within the capping inversion on the DDC sounding. A representative dry adiabat is labeled by Γ_d.

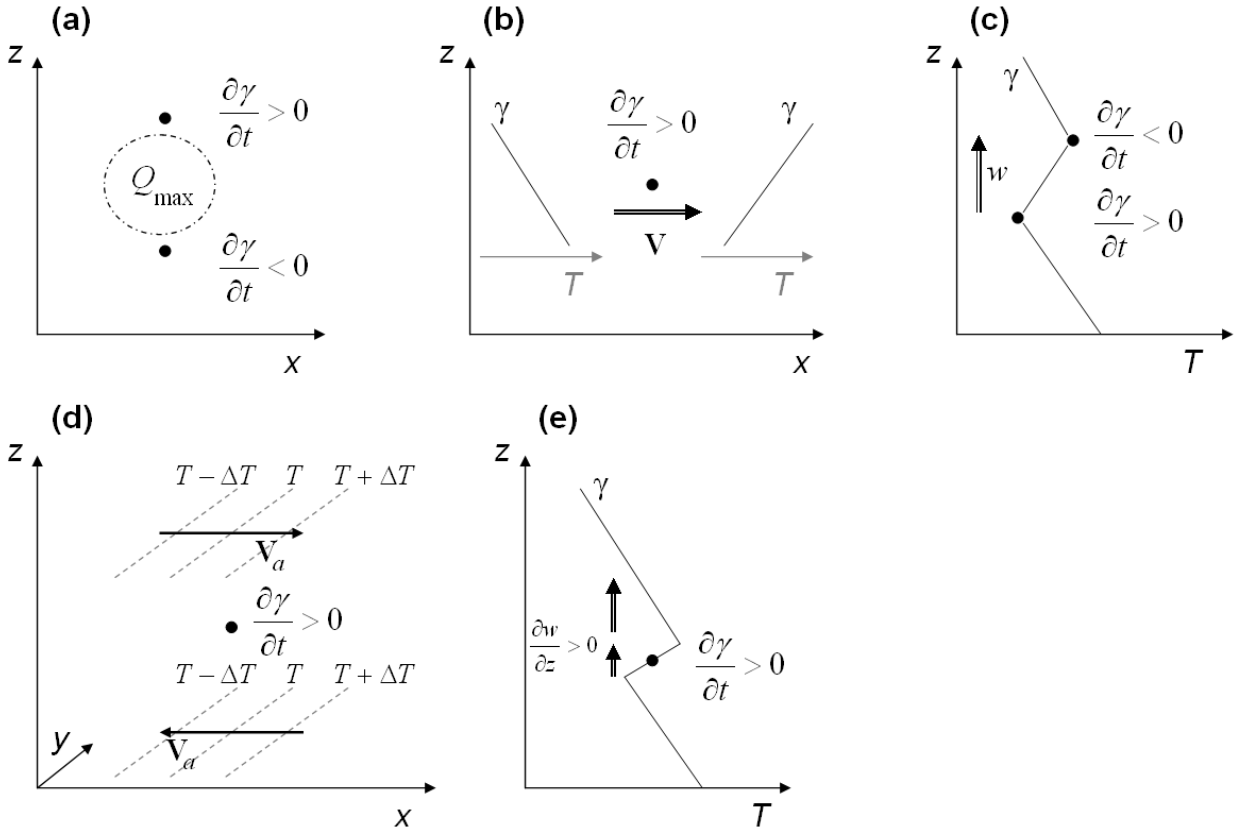

FIGURE 2. Illustration of the effect of physical processes on the local time rate of change of environmental lapse rate, γ. In (a), owing to a diabatic heating maximum, (b) due to horizontal lapse rate advection, (c) due to the vertical advection of lapse rate, (d) due to differential ageostrophic temperature advection, and (e) due to vertical stretching. The sense of the lapse rate tendency is shown at point locations.

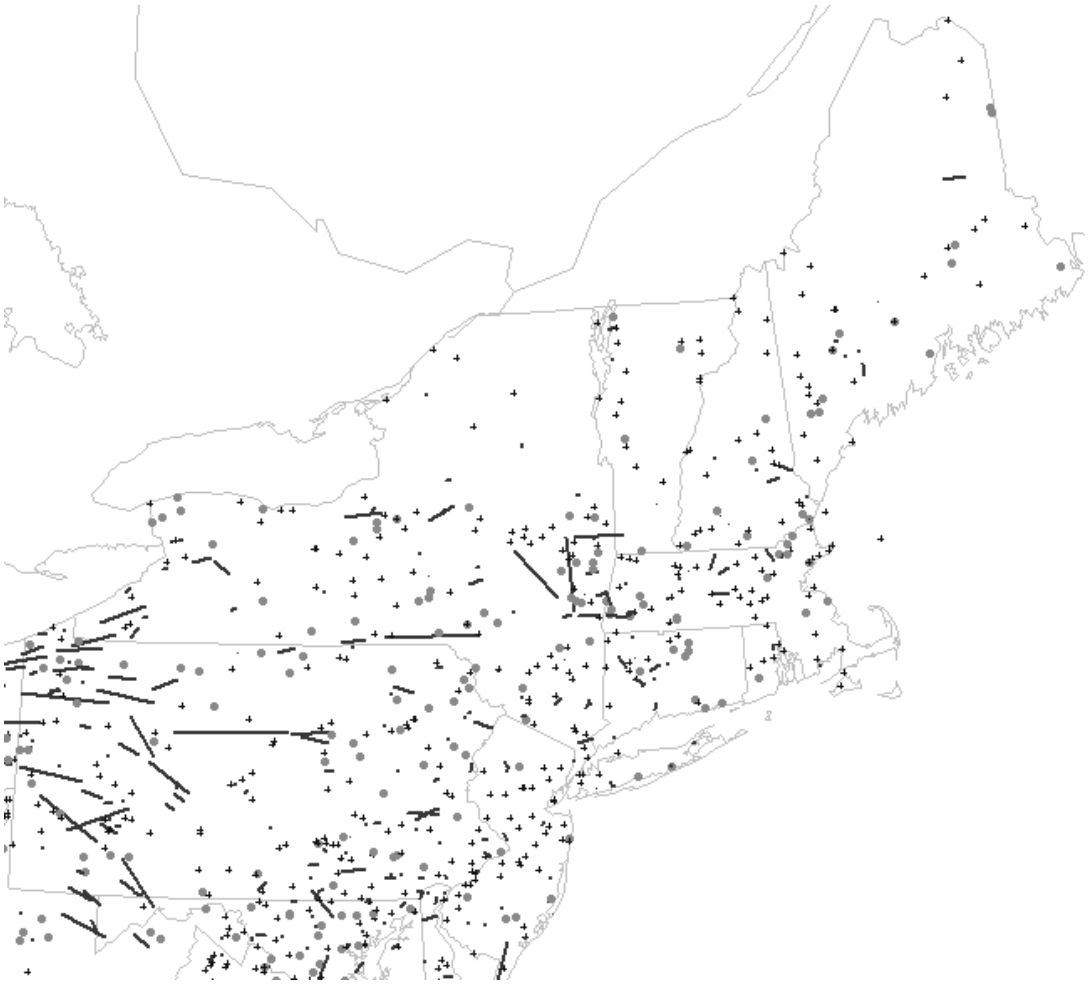

FIGURE 3. Plot of all significant severe weather reports over the Northeastern United States from May 1st through September 30th, 1970-2006. Dots and lines represent F2 or greater tornadoes, crosses represent measured convective wind gusts of 65 kts or greater, and circles show hail of 2 inches in diameter or greater.

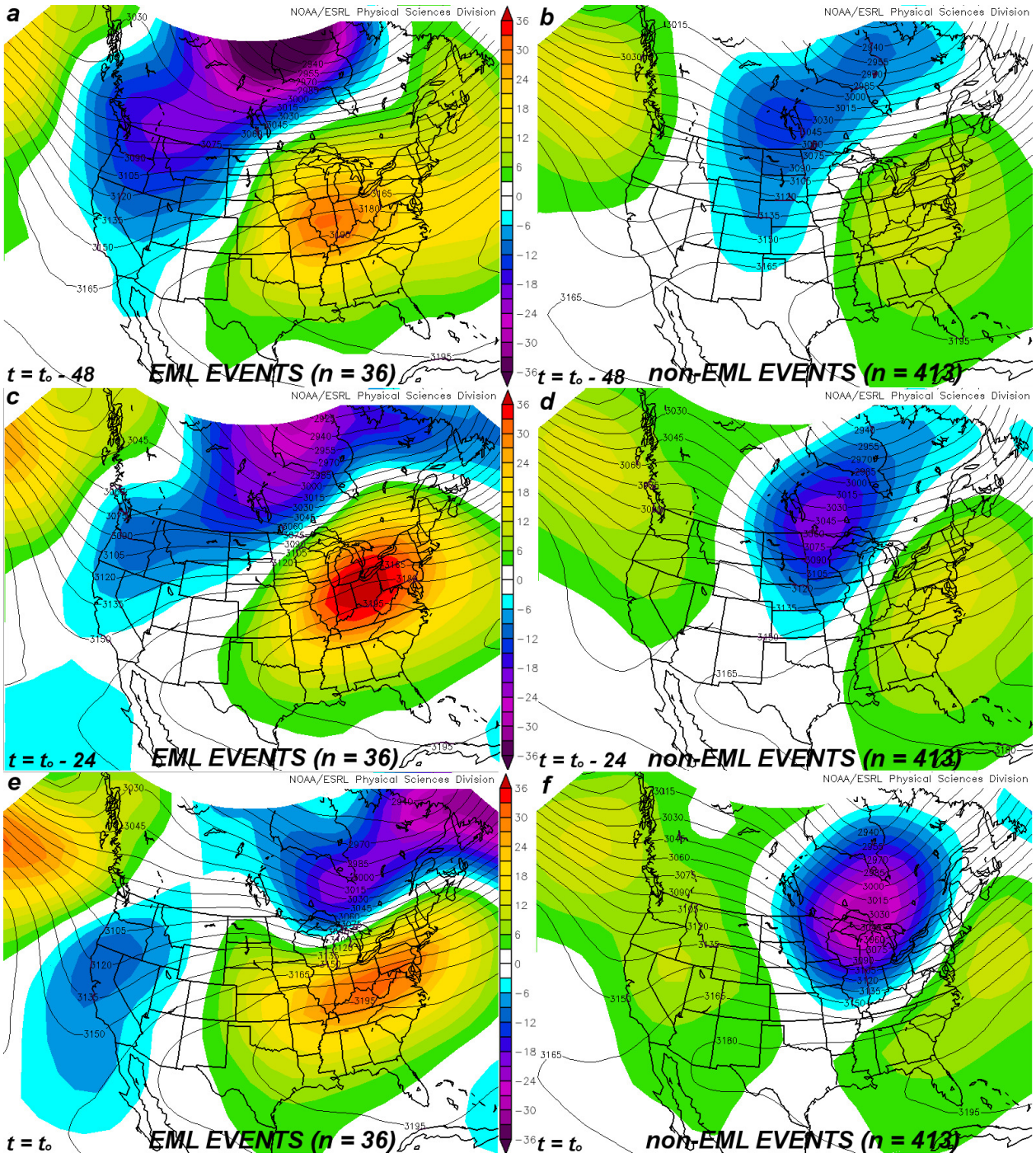

FIGURE 4. Composite analyses of the mean 700 mb geopotential height (solid contours) and 700 mb height anomaly (shaded) (versus 1968-1996 climatology) based on the NCEP/NCAR reanalysis dataset for all EML events (left column) and all SIG SVR non-EML events (right column). Time t_o corresponds to the 6-hourly sub-synoptic time step preceding the first significant severe weather report for each of n events listed. Composite panels a-b are valid at t_o – 48 h, panels c-d at t_o – 24 h, and panels e-f at t_o. The contour interval is 15 m and 3 m for the mean geopotential height and height anomaly analyses, respectively.

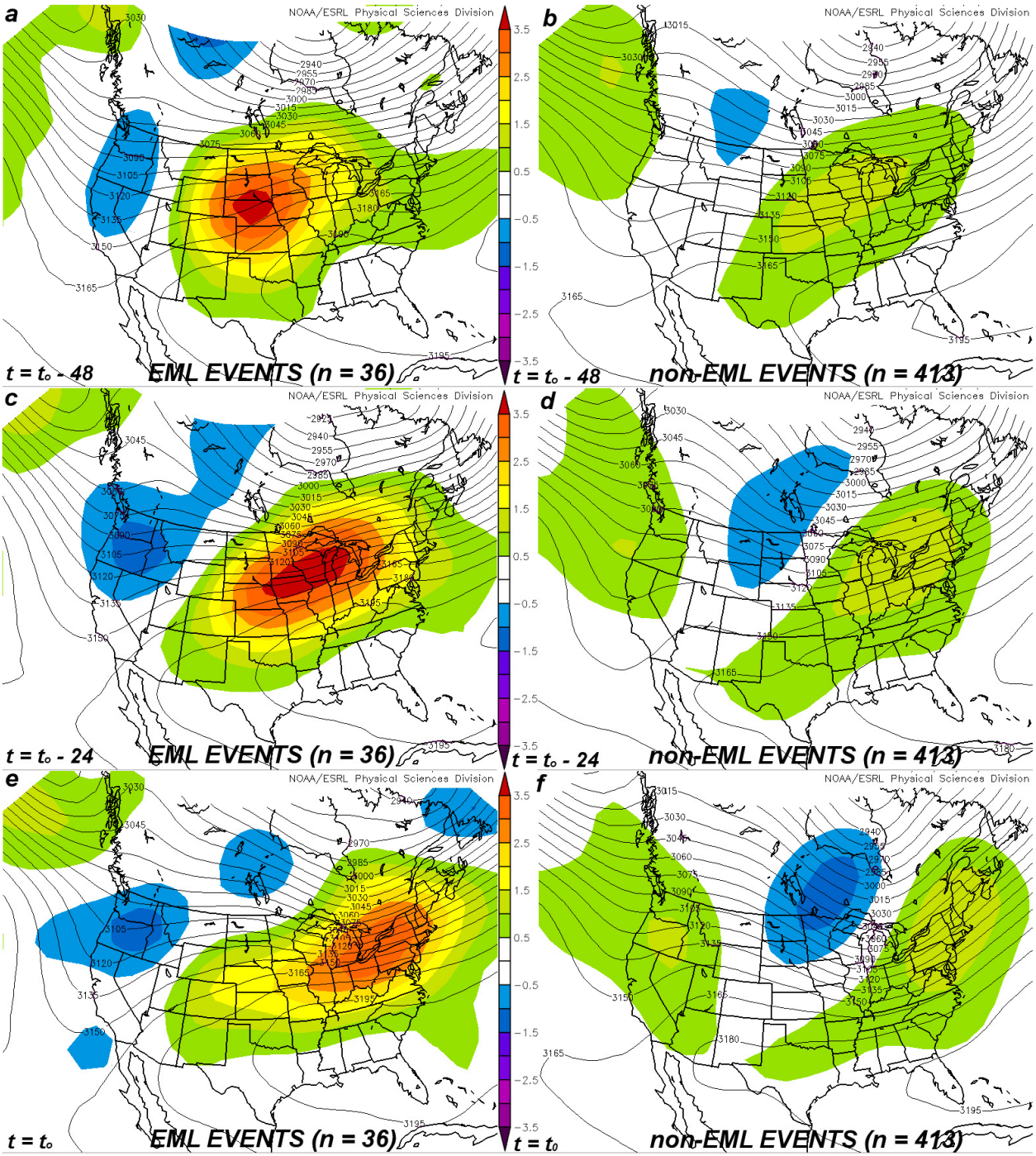

FIGURE 5. Composite analysis as in Fig. 4, except for 700mb temperature anomaly (shaded, 0.5 ^{o}C shading interval).

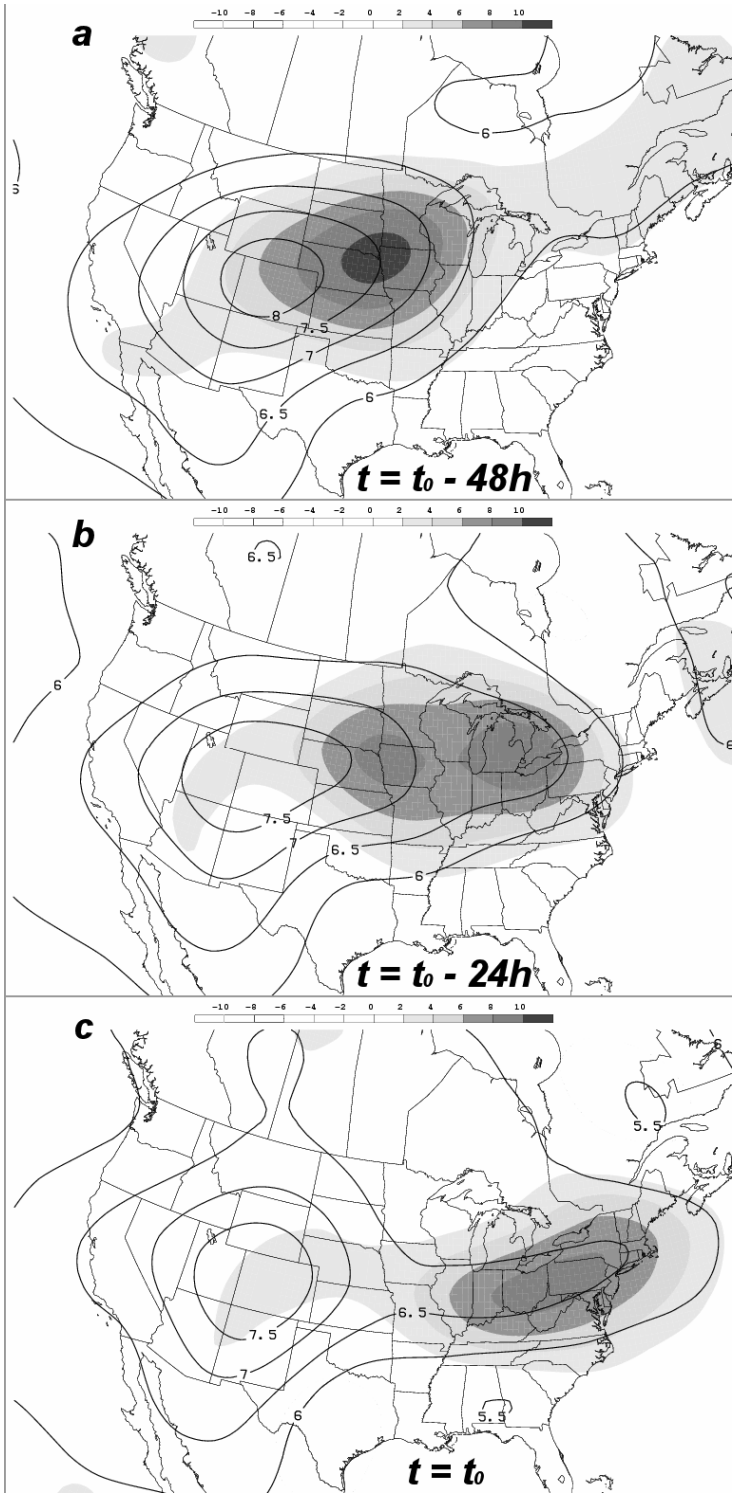

FIGURE 6. Composite 700-500mb mean lapse rate for all 36 EML events based on NCEP/NCAR Global Reanalysis data for (a) t_o – 48 h, (b) t_o – 24 h, and (c) at t_o. Solid lines represent γ with a contour interval of 0.5 ^{o}C km^{-1}. Shading represents 700-500mb lapse rate anomaly in tenths of degrees ^{o}C km^{-1} based on 1971-2000 climatological values. Contour interval for the lapse rate anomaly is 0.2 ^{o}C km^{-1}.

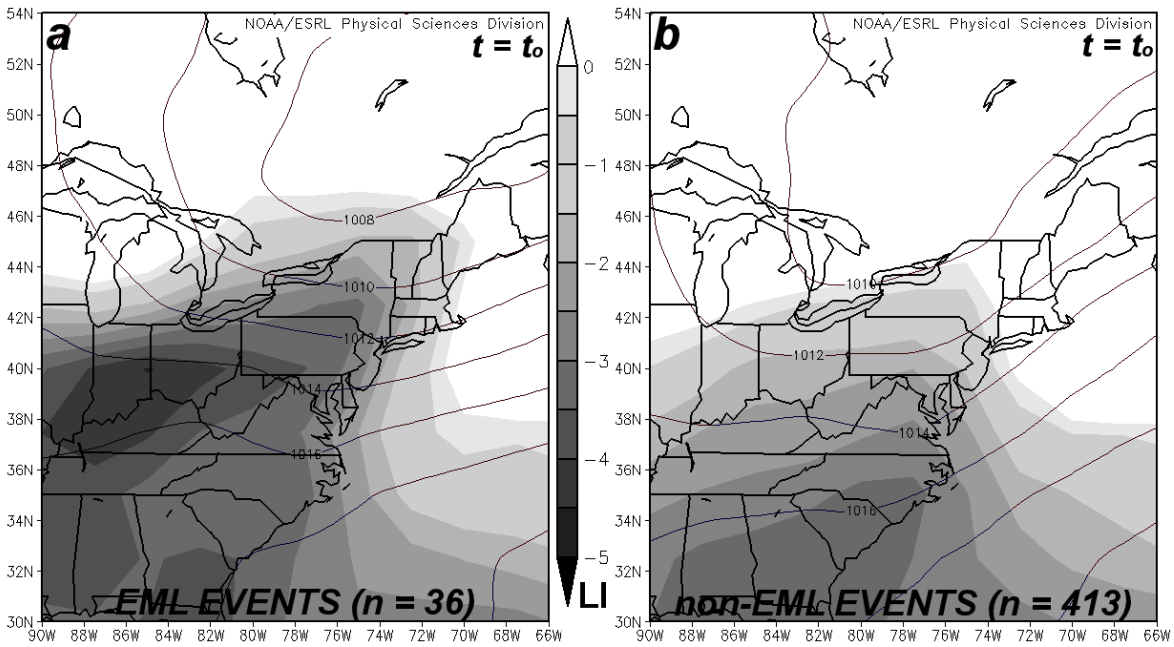

FIGURE 7. Composite mean 4-layer best lifted index (Celsius, shaded every 0.5 ^{o}C) and sea-level pressure (solid, isobars every 2 mb) for (a) EML events and (b) non-EML events. Time t_o corresponds to the 6-hourly sub-synoptic time step preceding the first significant severe weather report for each of n events listed.

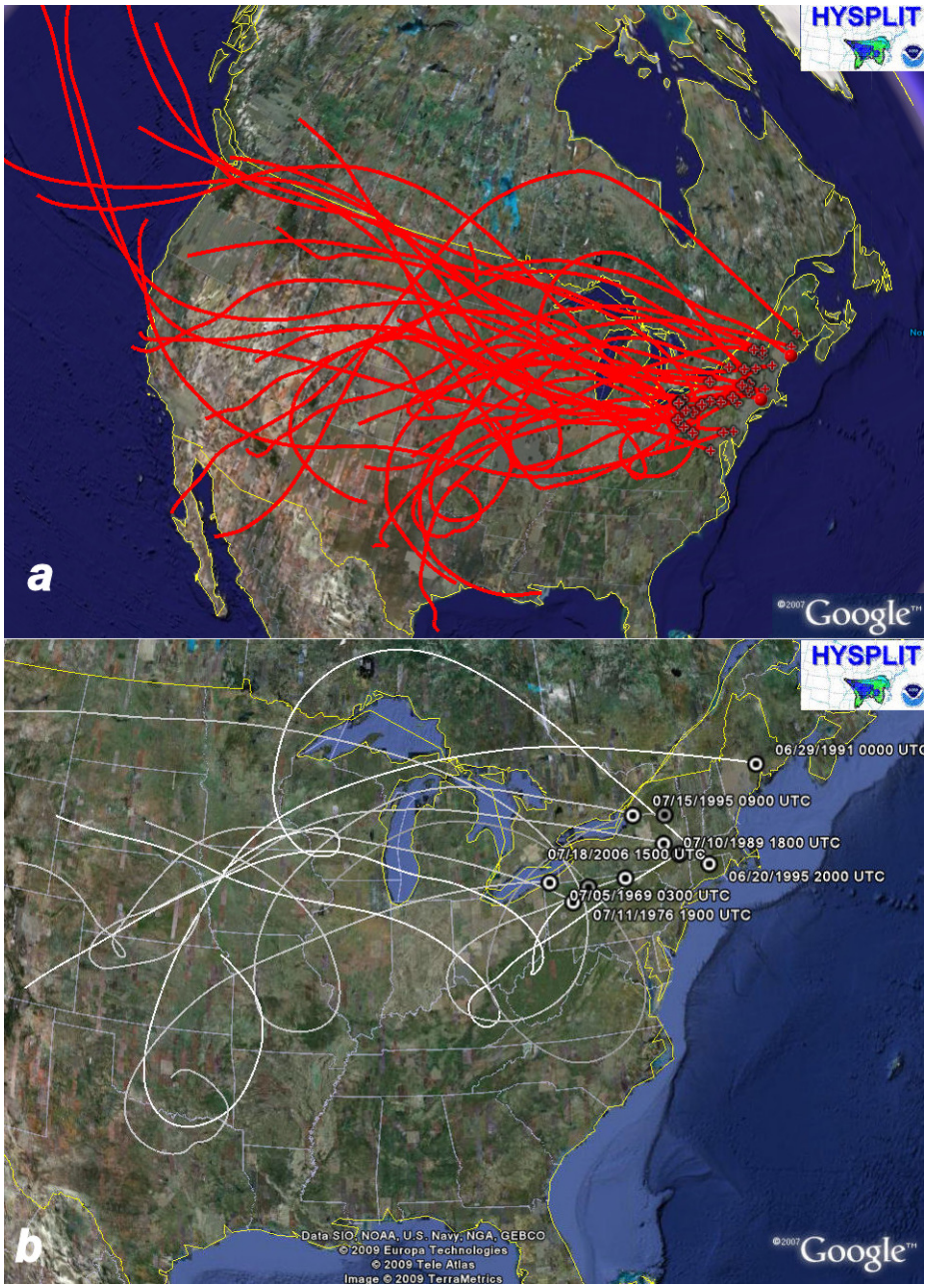

FIGURE 8. Backward 3-km AGL trajectories taken from the location of the first significant severe weather report (marked by circles) rounded to the nearest hour for (a) each of the 36 EML events, and (b) subset of ten trajectories exhibiting three-quarter or greater anticyclonic loops along their path. Each trajectory duration is 96 hours.

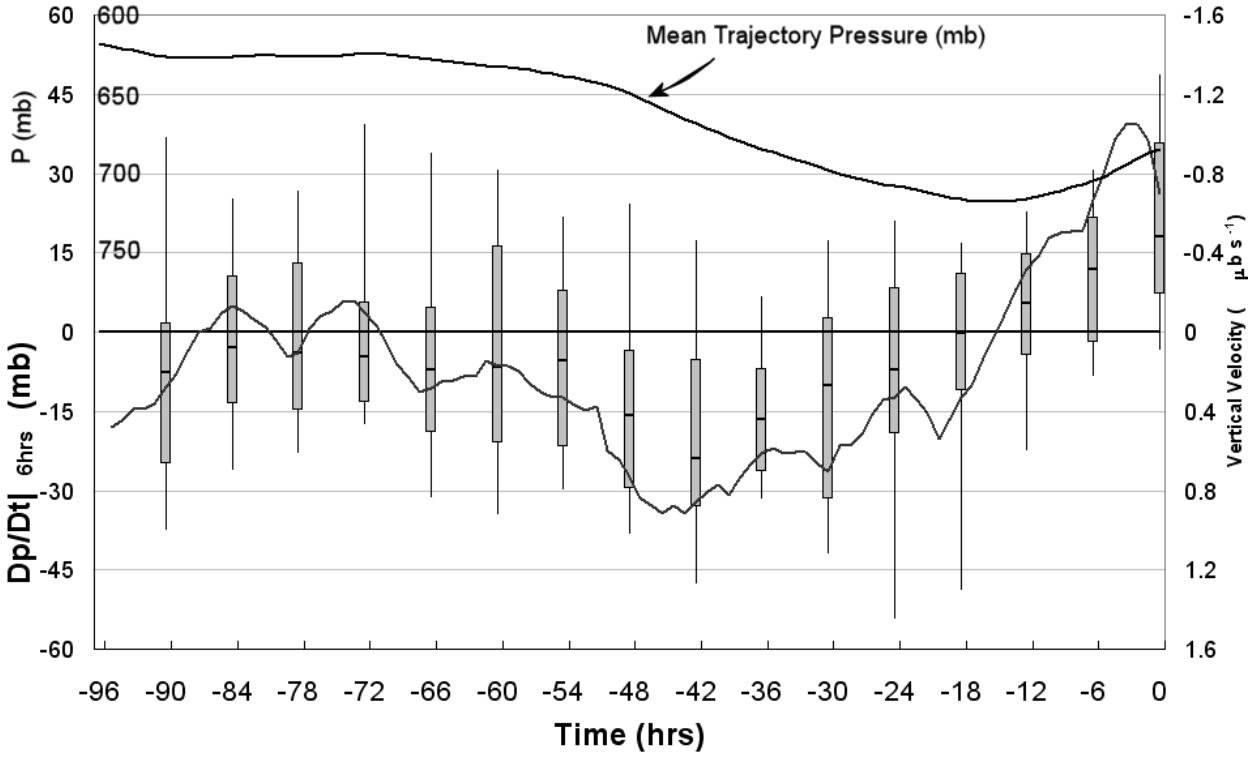

FIGURE 9. Time series analysis of 3-km AGL backward trajectories for the 36 EML events. Box-and-whisker graph shows 6-h pressure change following trajectory motion ($\left.\frac{Dp}{Dt}\right|_{6h}$, in mb) with scale on outside of left ordinate. Median pressure change is shown by black line within the box, the box encompasses 25th to 75th percentile pressure change, and ends of whiskers correspond to 10th and 90th percentile pressure change. Lines show time-height cross-section of mean backward trajectory pressure (mb, top line with scale on inside of left ordinate), and mean instantaneous vertical velocity (bottom line, scale on right ordinate). Time along abscissa corresponds to the number of hours before the first significant report. Results are from NOAA HYSPLIT model run on Global Reanalysis dataset.

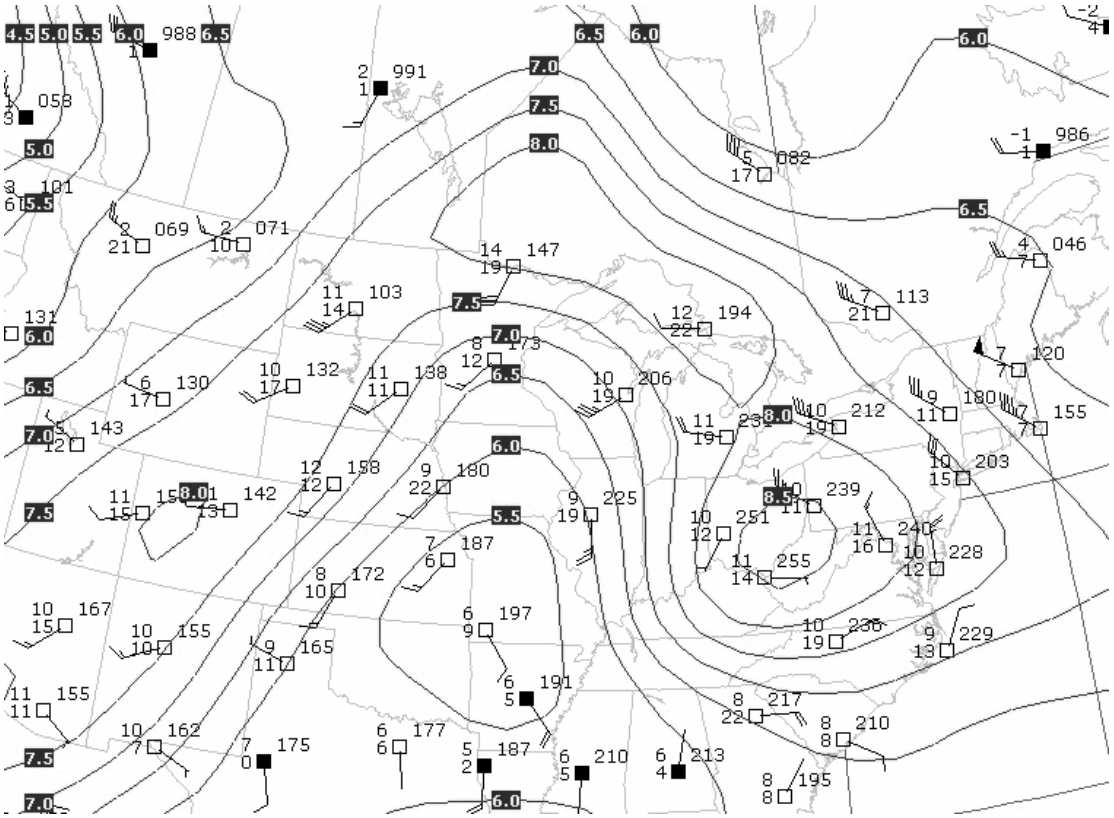

FIGURE 10. The 700 mb rawinsonde plot at 12 UTC 28 August 1973. Each full (half) barb is 5 ms^{-1} (2.5 ms^{-1}). The 700-500 mb mean lapse rate (^oC/km, solid lines every 0.5 degrees) is contoured.

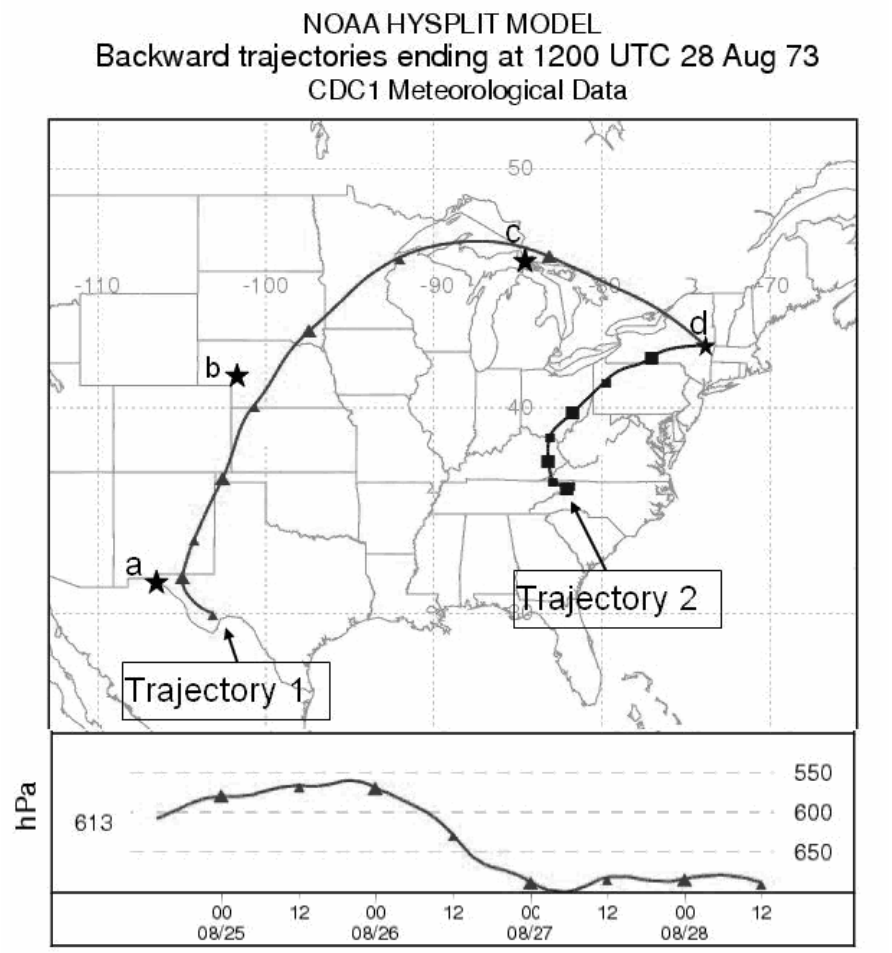

FIGURE 11. The HYSPLIT model 96-hour backward trajectory analysis (plotted every 12 hours) starting at Albany, NY at 12 UTC 28 August 1973. Trajectory 1 approximates the path of the EML plume in the middle troposphere, with time-height analysis shown in bottom panel. Trajectory 2 represents the path of the 2-m (surface) air parcel. Points a-d represent the rawinsonde locations utilized in Fig. 12.

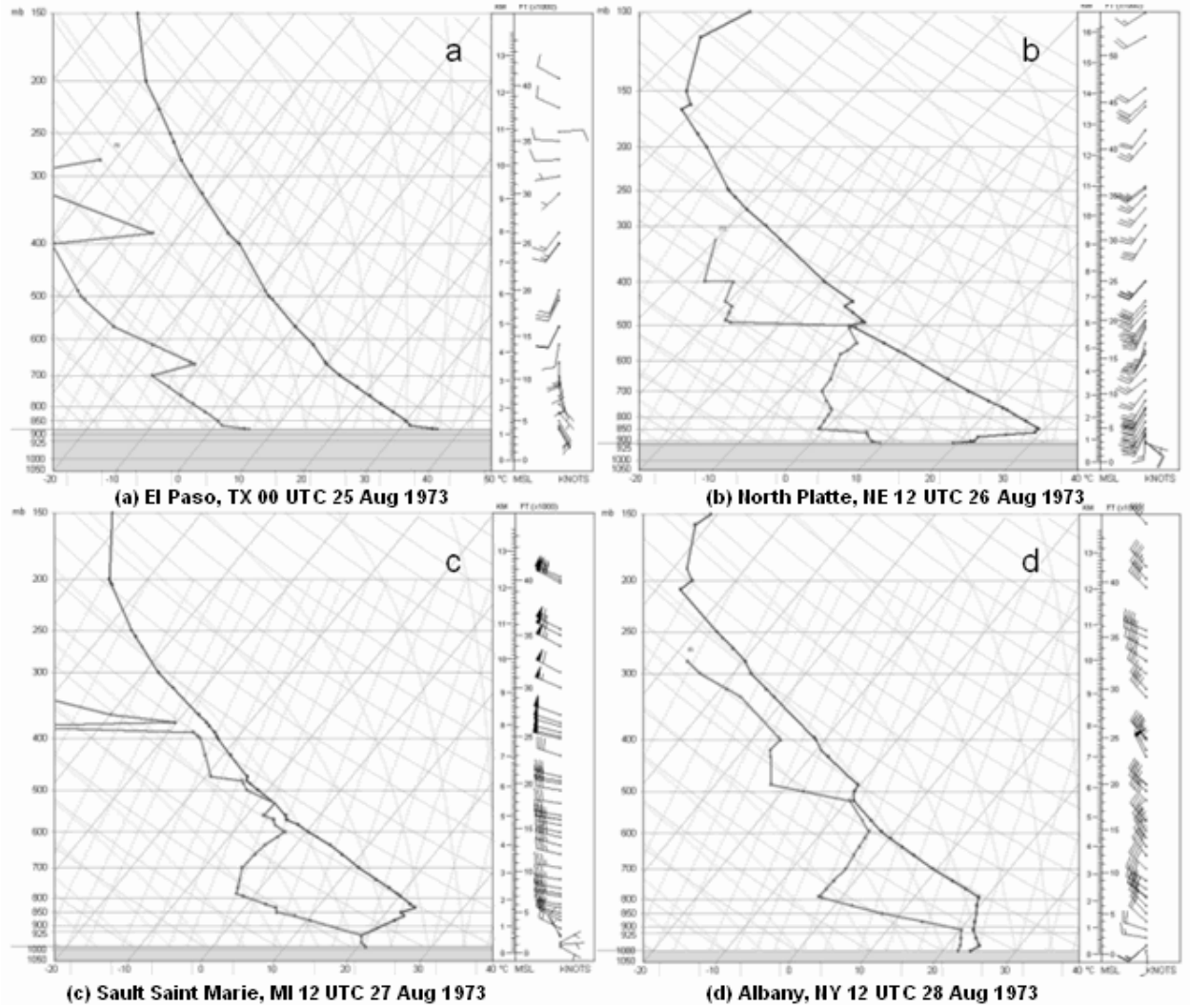

FIGURE 12. Soundings taken at points a through d along "Trajectory 1" in Fig. 11. The soundings are: (a) El Paso, TX 00 UTC 25 Aug 1973, (b) North Platte, NE 12 UTC 26 Aug 1973, (c) Sault Saint Marie, MI 12 UTC 27 Aug 1973, and (d) Albany, NY 12 UTC 28 Aug 1973.

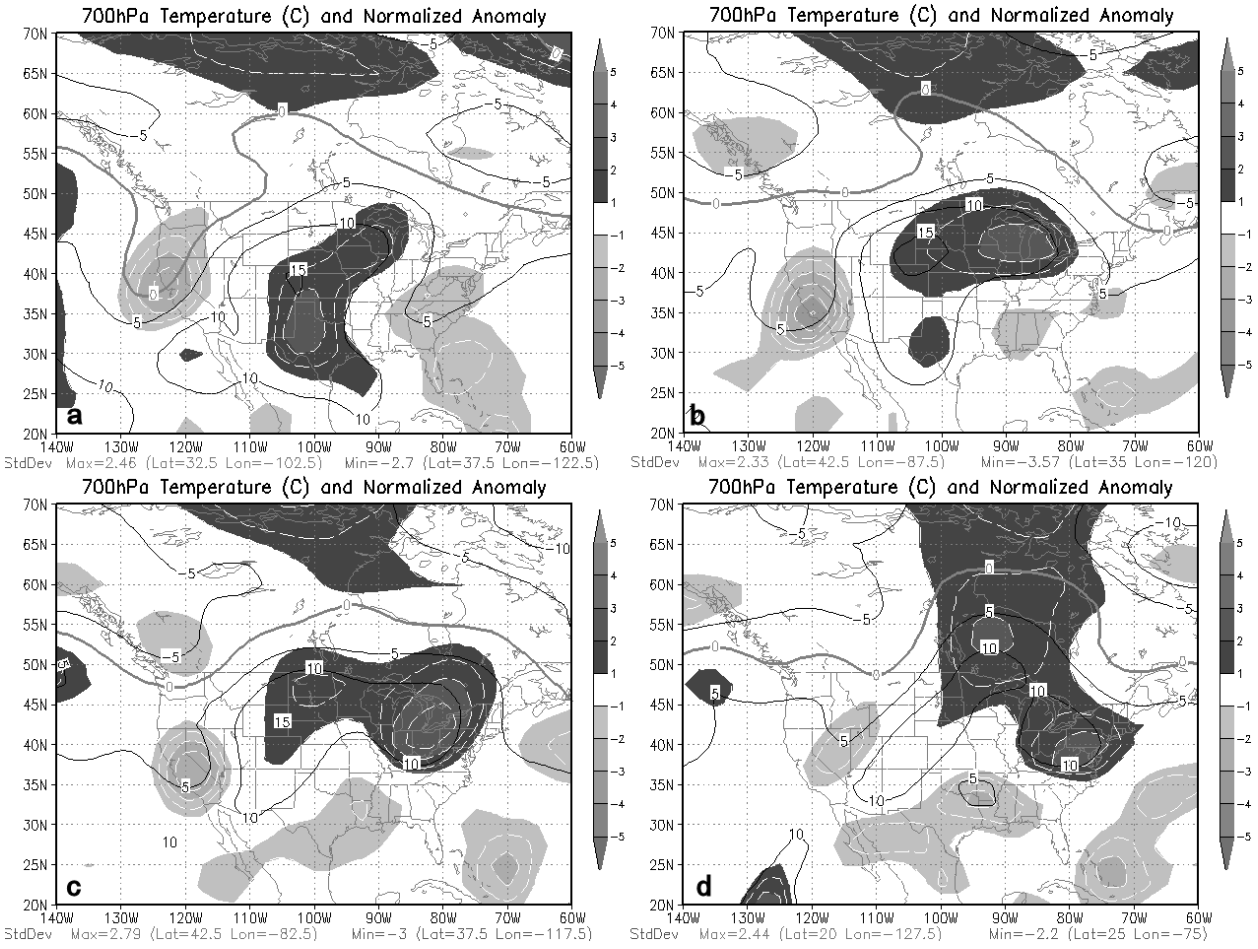

FIGURE 13. The 700 mb temperatures (°C, solid contours) and anomalies (standard deviations from the 1961-90 climatological mean, shaded) derived from the NCEP/NCAR reanalysis at (a) 12 UTC 25 Aug 1973; (b) 12 UTC 26 Aug 1973; (c) 12 UTC 27 Aug 1973; (d) 12 UTC 28 Aug 1973.

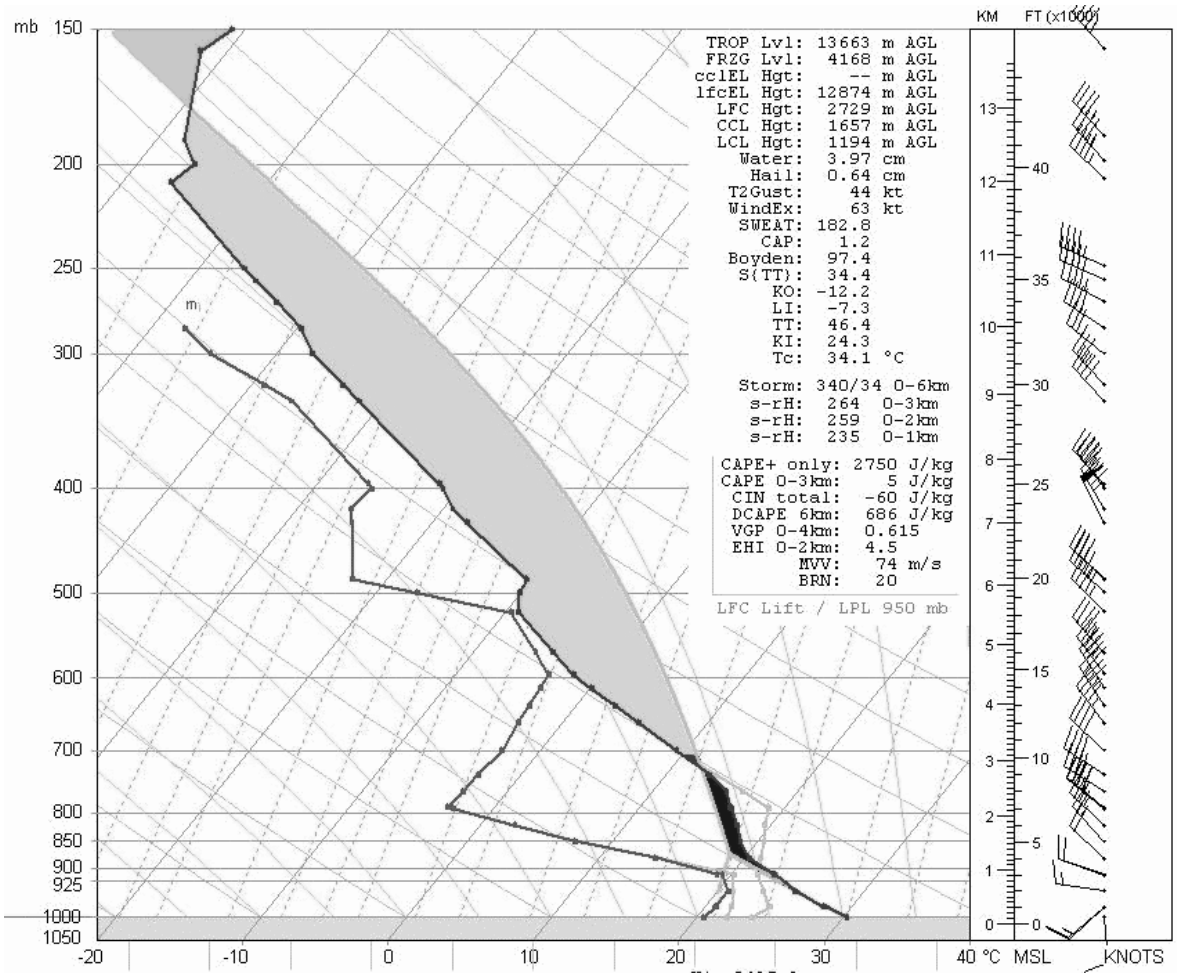

FIGURE 14. The 28/12 UTC ALB sounding modified for 28/20 UTC temperature and dewpoint from the surface observation at ALB. Mixed layer CAPE and CIN are shaded.

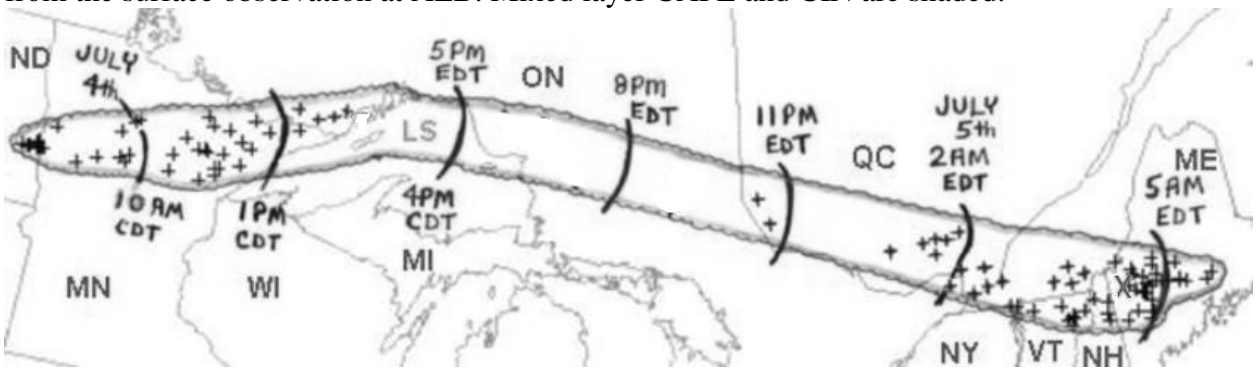

FIGURE 15. Area affected by the 4-5 July 1999 derecho (scalloped line) with isocrones of the leading edge gust front at 3-h intervals (curved lines). Crosses indicate locations of wind damage or estimated wind gusts above severe limits (25 ms^{-1} or higher). (Analysis provided by Bob Johns)

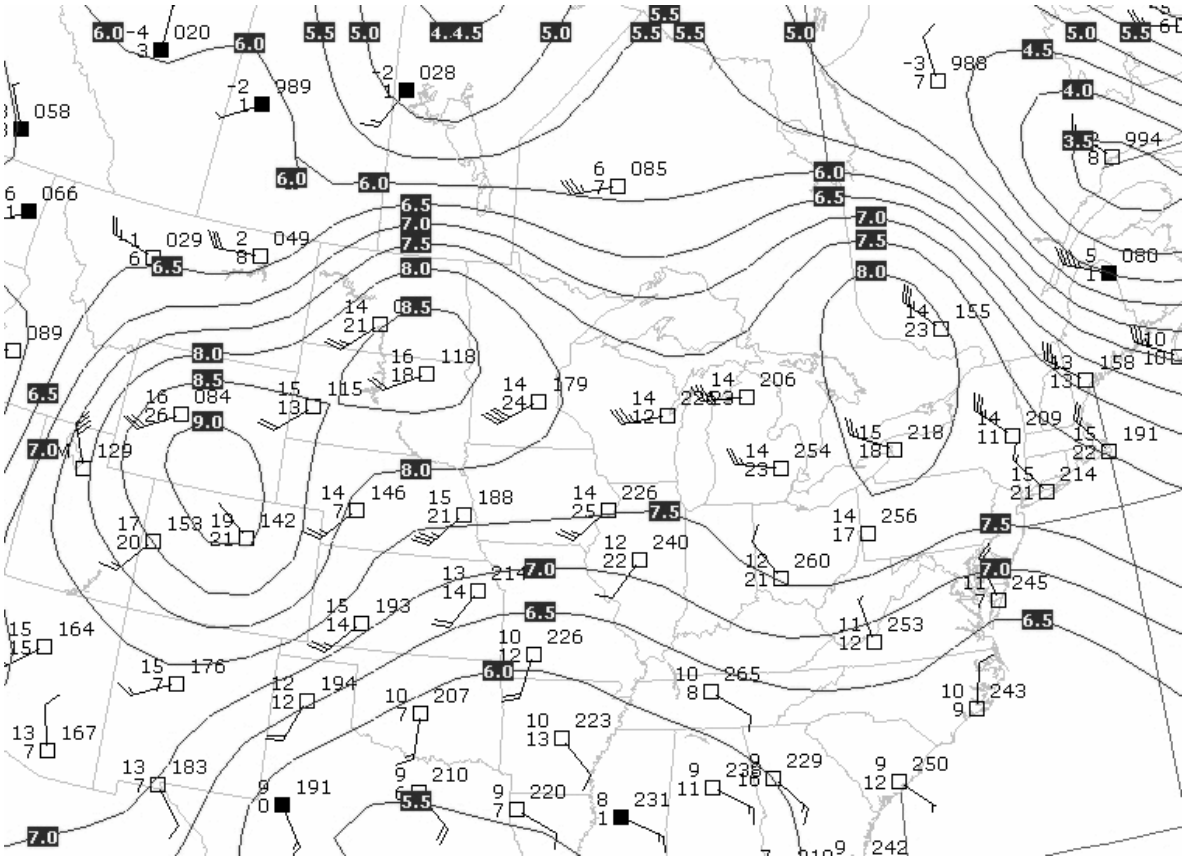

FIGURE 16. As in Fig. 10 except at 00 UTC 5 Jul 1999.

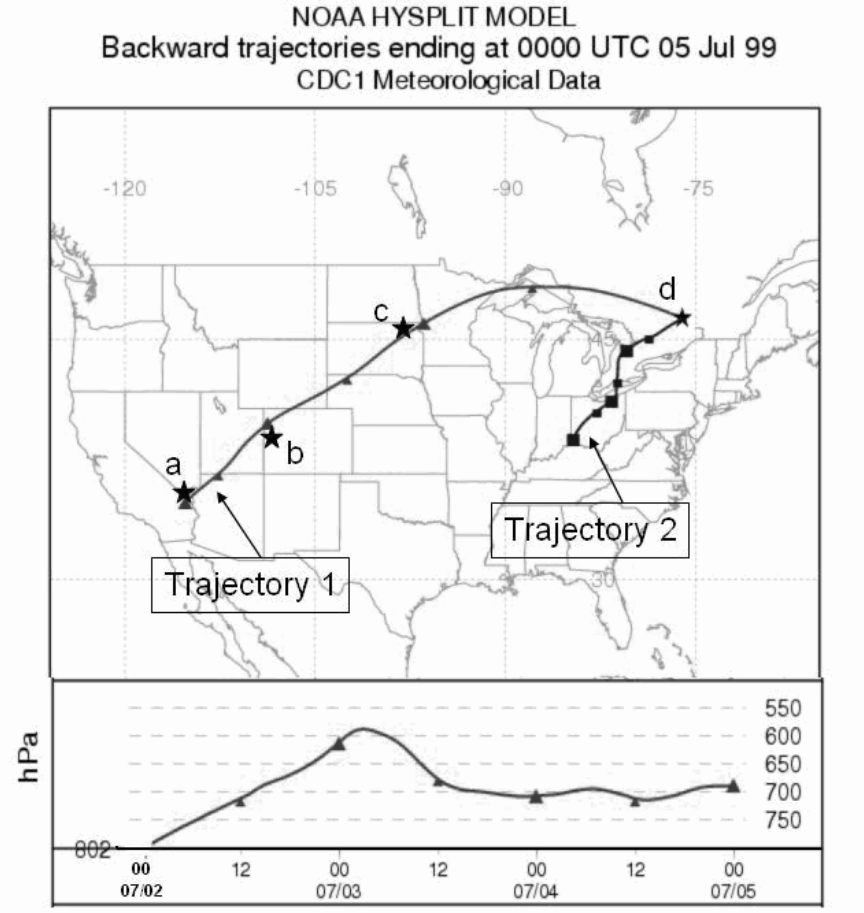

FIGURE 17. As in Fig. 11 except starting from Maniwaki, Quebec at 00 UTC 05 Jul 1999. Points a through d represent the rawinsonde locations shown in Fig. 18.

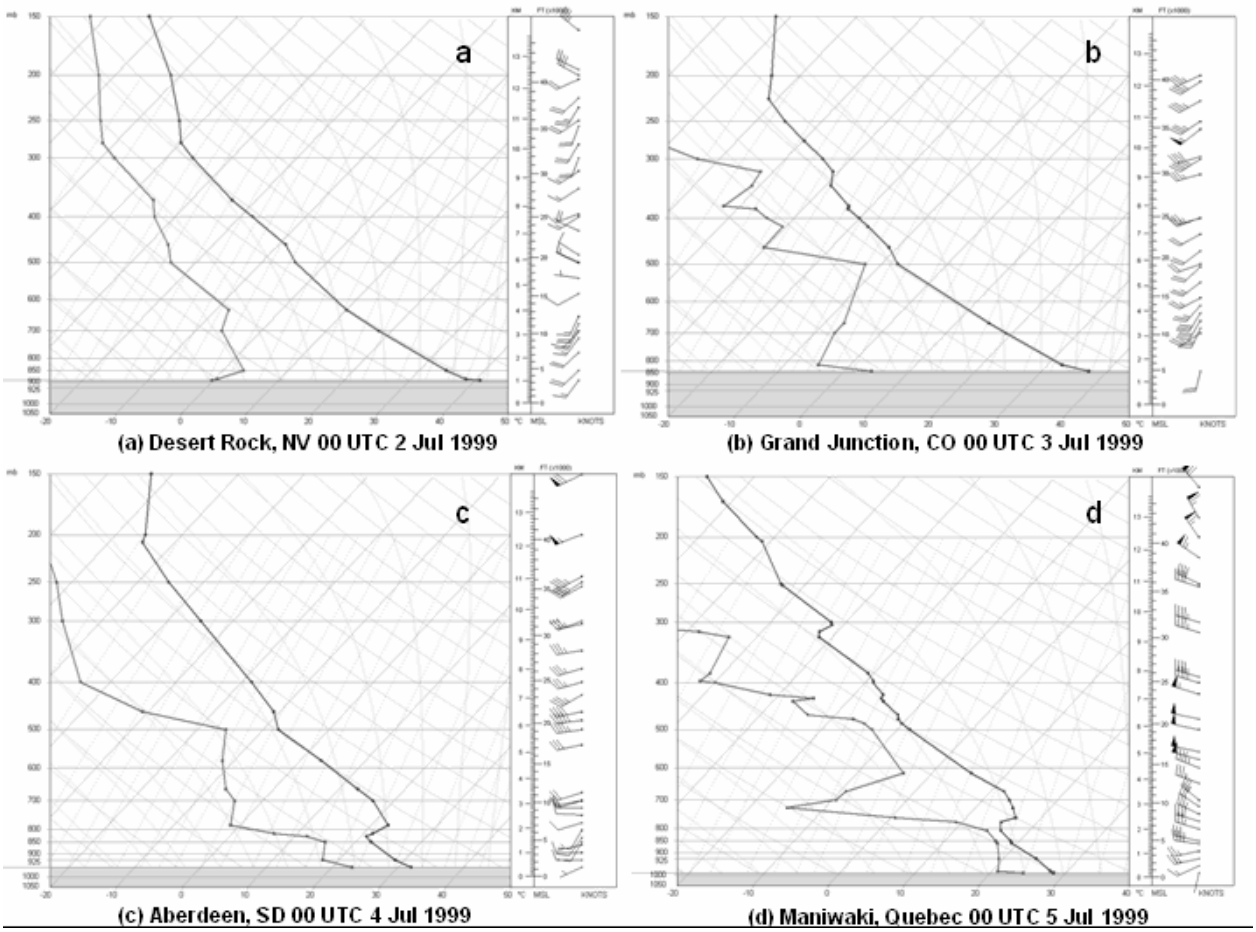

FIGURE 18. Observed soundings along Trajectory 1 in Fig. 17 at (a) Desert Rock, NV 00 UTC 02 Jul 1999; (b) Grand Junction, CO 00 UTC 03 Jul 1999; (c) Aberdeen, SD 00 UTC 04 Jul 1999; (d) Maniwaki, Quebec 00 UTC 05 Jul 1999.

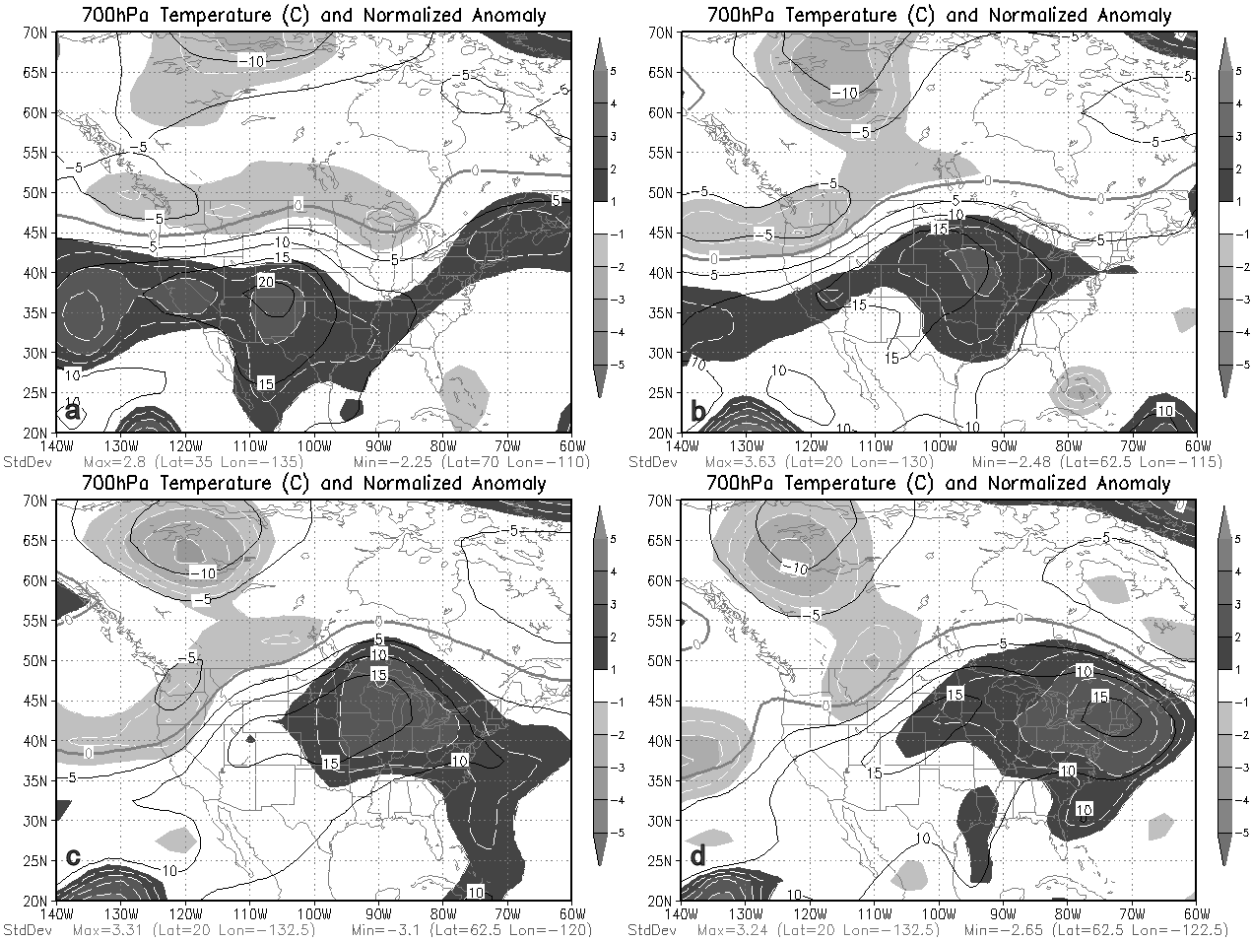

FIGURE 19. As in Fig.13 except at (a) 06 UTC 2 Jul 1999; (b) 06 UTC 3 Jul 1999; (c) 06 UTC 4 Jul 1999; (d) 06 UTC 5 Jul 1999.